Vigilada Mineducación

Design and Analysis of a Wave Energy Converter of Point Absorber Type for the Energy Extraction from the Waves

Carlos Enrique Pimienta Martínez

Universidad del Norte
Department of Electric and Electronics Engineering
Barranquilla, Colombia
2019

Design and Analysis of a Wave Energy Converter of Point Absorber Type for the Energy Extraction from the Waves

Thesis presented to the Department of Electric and Electronics Engineering of Universidad del Norte as a partial requirement to opt for the title of Master of Science in Electrical Engineering

Carlos Enrique Pimienta Martínez

Advisor:
Ingrid Oliveros Pantoja, PhD

Research Line: Energy and Environment
Electrical Power Systems Research Group (Spanish abbreviation: GISEL)
Department of Electric and Electronics Engineering
Universidad del Norte
Barranquilla, Colombia
2019

Dedicated to my father and son.

Acknowledgements

First of all, to God, who gave me the wisdom and the strength to better deal with my Master's project.

My wife and son, people who charged me with energy every time I felt tired. They waited for me every weekend to give me a hug, a kiss and words of encouragement.

My parents and brother, essential people in my life who gave me their support from start to finish. They never doubted me, and I will always be eternally grateful to them.

My advisor Ingrid Oliveros and my co-advisor Javier SanJuan, who believed in my work and my abilities to develop this great work.

My friends Lucho, Juan, Jose, Ever and Nathalia, who supported this great project and gave their time to build it.

My Professor Oscar Alvaréz who dedicated a great part of his time and provided great support in everything related to the project.

And all the people who gave me part of their time to help me. I will be eternally grateful.

Abstract

The generation of electric power from ocean waves has been in constant technological growth during the last decades, for being a clean source of abundant and renewable energy. However, the existing systems are extensive in size and cost. Thus, in this thesis, a design methodology for the construction of a wave energy prototype is developed. The proposed device is a slider-crank mechanism connected to a spherical buoy. The buoy, situated on the surface of the water, takes advantage of the vertical movement of the waves converting their oscillation movement into a rotational motion that actuates over the shaft of the armature coils within the generator to obtain electric power. The design of the mechanical components was conducted by the application of the principle of Virtual Work and D'Alembert, which allowed the determination of the dynamical model of the system; then, using these results, the mass and inertia of each element were obtained by an optimization procedure using the Optimization Toolbox of Matlab. Lastly, the results of the mathematical model were validated by experimentation in a scaled prototype of the dispositive.

Nomenclature and Abbreviations

Abbreviations

Symbol	Meaning
$DEDS$	Direct Electrical Drive Systems
$DEDS$	Direct Mechanical Drive Systems
FT	Fourier Transform
OWC	Oscillating Water Column
$PMDC$	Permanent Magnet DC
SDP	Spectral Density of Power
WEC	Wave Energy Converter

Nomenclature Chapter

Symbol	Meaning	Unity SI
A	Added Mass	
a_1	Acceleration of the Crank	m/s^2
a_2	Acceleration of the Connecting Rod	m/s^2
B	Damping coefficient	
C	Buoy Hydrostatic Stiffness	
c	Phase Speed	m/s
E	Variance Density	m^2/s
F	Heave Excitation Force	N/m
F_b	Buoyancy Hydrostatic Force	N/m
F_d	Damping Force	N/m
F_{optm}	Minimum Average Input Force	N/m
F_r	Radiation Force	N/m

f	Frequency	Hz
g	Gravitational	Hz
H	Wave Height	m
I_1	Inertial Moment of the Crank	$kg.m^2$
I_2	Inertial Moment of the Connecting Rod	$kg.m^2$
h	Amplitude	m
k	Wavenumber	kg/m^2
L_1	Length of Crank	m
L_2	Length of Connecting rod	m
L_3	Center Mass Buoy Position	m
M	Inertial Moment of the Flywheel	$kg.m^2$
M_1	Mass of the Crank	kg
M_2	Mass of the Connecting Rod	kg
m_a	Semi-submerged Buoy Mass	kg
m_b	Buoy Mass	kg
R	Radiation Coefficient	
R_v	Viscous Force Coefficient	
R_f	Friction Force Coefficient	
T	Period	s
z	Buoy Center of Gravity Displacement	m
$\dot{z}$	Buoy Velocity	m/s
α_1	Angular acceleration of the Crank	m/s^2
α_2	Angular acceleration of the Connecting Rod	m/s^2
β_1	Angle of the Crank	$^\circ$
β_2	Angle of the connecting rod	$^\circ$
δ_{x_1}	Displacement of the Mass Center of Crank	m
δ_{x_2}	Displacement of the Mass Center of Connecting Rod	m
δ_{θ_1}	Displacement between Crank and Connecting Rod	$^\circ$
δ_{θ_2}	Displacement between Connecting Rod and buoy	$^\circ$

δ_q	Displacement of the Buoy	m
α_1	Angular Acceleration of the Crank	rad/s
α_2	Angular Acceleration of the Connecting Rod	rad/s
ε_r	Radiation Resistance Coefficient	
ρ_b	Buoy Density	kg/m^3
ρ_w	Sea Water Density	kg/m^3
ω	Angular Frequency	rad/s
λ	Wavelenght	m

List of Figures

List of Tables

Contents

1. Introduction

The increase in energy demand and the challenges for reducing environmental pollution has led to the search for new sources of energy. Such is the case of the energy contained in the ocean in the form of waves. The waves are formed due to the influence of the wind and the sun, however, when comparing the density in energy production of the waves with the solar or eolic energy, the density production of the waves is fives and ten times higher, respectively[1]. Besides, ocean waves have a consistent activity cycle and its behaviour is more estimable, which makes it an energy source with more significant potential to reduce the energy crisis [2, 3].

According to studies done to analyze the energy potential of natural resources, different organisms have focused on the use of ocean energy, because of its energy potential of approximately 8,000-80,000TW/year [4]. A clear example of countries researchers and developers of technology for the use of this energy are New Zealand, United States, United Kingdom (includes: England, Scotland, Northern Ireland) [5], among others, which have been improved the use of this resource.

Given the great source of energy that comes from the oceans, there is a great variety of alternatives for the use of these natural resources. Among the types of electric power generation from maritime resources are [6]: Wave energy, which is characterized by the use of the amplitude and frequency of the waves. Tidal energy focuses on the kinetic energy of the current water motion. Temperature gradient obtains the energy from the thermal differential generated by the solar radiation over the upper oceanic layers. Finally, saline gradient takes advantage of the differential of saline concentration between the water of the oceans and rivers.

According to the different studies carried out on the analysis of energetic theoretical potential around the world, we find that the energy wave possesses approximately 32,000 TWh/year [7], including the continental platforms. Tidal energy has a global energy potential estimated of approximately 150TWh/year [8]; temperature gradient has an annual net power potential of about 30 TWh/year [9]; saline gradient has an energetic global potential of 1,650 TWh/year [7]. However, tidal and the wave energy

are the two ocean energy technologies with the more potential to produce electricity, and it is expected by researchers that, in the short-medium term, both will become commercially viable [10]. From this perspective, this research focuses on the study of wave energy converters (WECs).

According to state of the art, WECs are classified by its size and the nearby wave characteristics [11]. Such classification is the following: attenuator, point absorber, pressure differential, oscillating wave surge, oscillating water column and overtopping [12]. However, the advantages of point absorber in comparison to the others converters are the possibility to absorb the wave energy in any direction. The design is simple, small and its installation and maintenance are easier to make [13].

Among the studies carried out on this type of converter are [14, 15]: Direct Mechanical Drive Systems (DMDS), Direct Electrical Drive Systems (DEDS) and Hydraulic Devices Systems (HDS). The DMDS uses the oscillating movement of the buoy, because of the interaction with ocean waves, to obtain electrical energy by the utilization of a mechanical system [16]. In contrast, The DEDS take advantage of the buoy displacement by moving a set of permanent magnets inside a linear electric generator [17]. Finally, HDS, in a similar fashion than DEDS, utilizes the buoy motion to drive hydraulic actuators that compress a fluid that is ultimately used to actuate an electric generator [18]. However, due to the low efficiency of HDS, and the low energy absorption of DEDS, the DMDS have been in constant development due to its high conversion efficiencies [3, 14].

Nowadays, due to the challenges that arise with DMDS, the researchers have focused on finding alternatives that will reduce the Levelized Cost Energy of Electricity (LCOE) of wave energy and be more competitive compared to other renewable energy resources [19]. Thus, to minimize the cost of DMDS, researchers have focused on the generation of mechanisms with a more simple design. Therefore, in this master's thesis proposes a methodology for the design of a point absorber converter of slider-crank type using the D'Alembert principle to simulate the relation between the forces and inertias of the system, to ultimately optimize the dispositive. The results of the optimization were validated through the construction of a prototype to laboratory scale. The conceptual design can be seen below in Figure **1-1**.

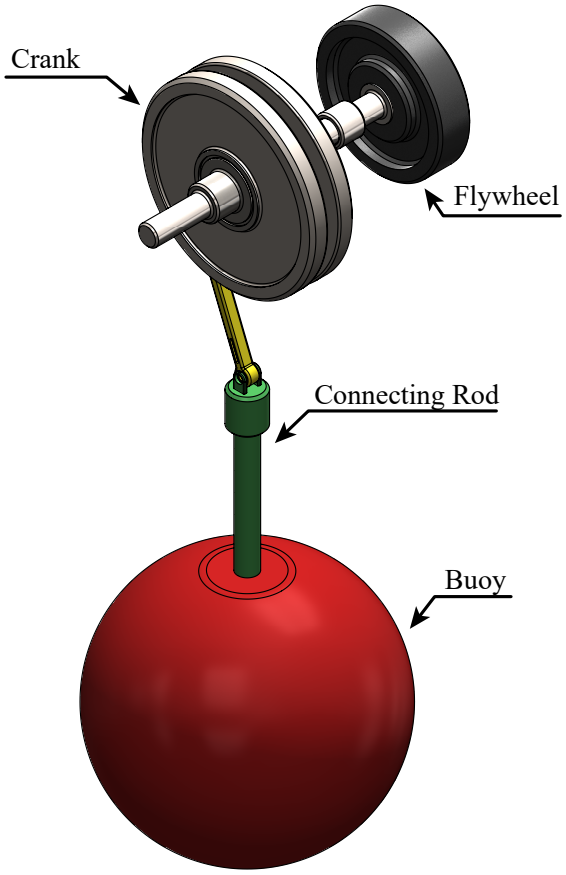

Figure 1-1.: The slider-crank: Design concept.

1.1. Objectives

This investigation project will focus on the design and build of a WEC system that will be used to generate electricity. In this master dissertation, it will apply a numerical study and experimental modeling. The aim is to know the operation of WEC mechanism and produce electric energy. From the above, it is described by a set of objectives, divide into general and specific objectives:

1. General objectives
    - To design and analyze a mechanism for a wave energy converter of type point absorber for energy generation from the waves.
2. Specific objectives
    - To model the wave energy converter of point absorber type using wave data and buoy geometry.
    - To analyze the forces of the buoy associated with the hydrodynamics of the wave.
    - To determine the voltage and current ratio generated by the wave energy converter when interacting with the wave.
    - To build the wave energy converter at laboratory scale for validation.

2. State of the Art

2.1. Wave Energy

The waves are born from the wind, dependent on the temperature, and pressure differential on the Earth's surface caused by the distribution of solar energy [20]. Among the main characteristics, we find that this natural source possesses kinetic and gravitational energetic potentials, which depart from the height and period of the wave [6]. Drew et al.[21] reviews the different benefits that can be obtained from wave energy, compared to other renewable sources such as solar or wind, such as:

1. Among the renewable energy source, the ocean waves have the highest energy potential. Waves are created by winds, which in turn are generated by solar energy. Solar energy intensity usually is 0.1–0.3kW/m^2 horizontal surface and this represents an average power flow intensity of 2–3kW/m^2 of the wave.

2. Low environmental impact potential.

3. The energy losses in the wave are minimal despite the long distances they travel.

4. The wind and solar power devices can generate power 20–30 percent of the time, compared to 90 percent produced by wave power technology.

Globally, the wave power distribution Figure **2-1**, shows the different zones with wave energy potential around the world, where the northern and southern hemisphere has more power. Thus, all of this has generated different estimates of the exploitable amount of wave energy. Gunn et al. [22] says the world wave average power resource is among in the range values of 2 or 3TW, meaning a theoretically available energy resource between 17,520 and 26,280TWh. The importance of this value born due to the compared to the overall world energy consumption in 2017, equal to 22,016TWh [23]. This noticeable value, makes this resource interesting to be explored.

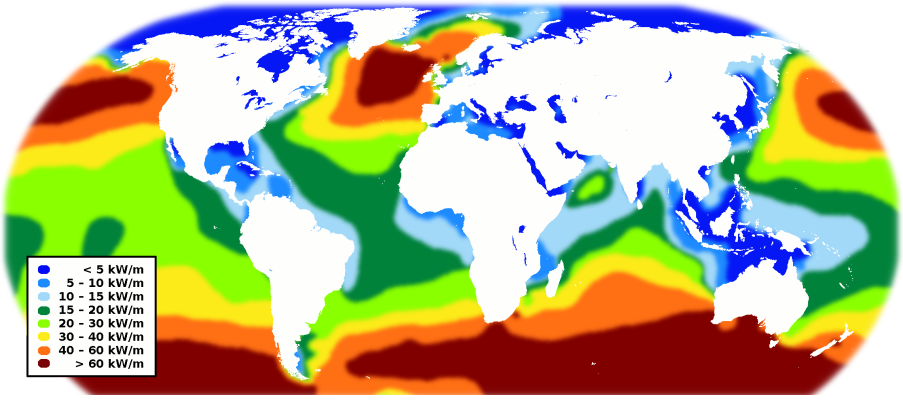

Figure 2-1.: Wave Power Level Distribution [24].

2.2. Wave Energy Converters Classification

One of the challenges to be solved in a WEC is extracting power from the sea surface with force. French [25] mentions that the classification of converters can be of different ways, depending on their main operation, their distance to the coast and the mechanical dimensions which are related to the wavelength parameter. In the next Figure **2-2** reported some prototypes for each technology.

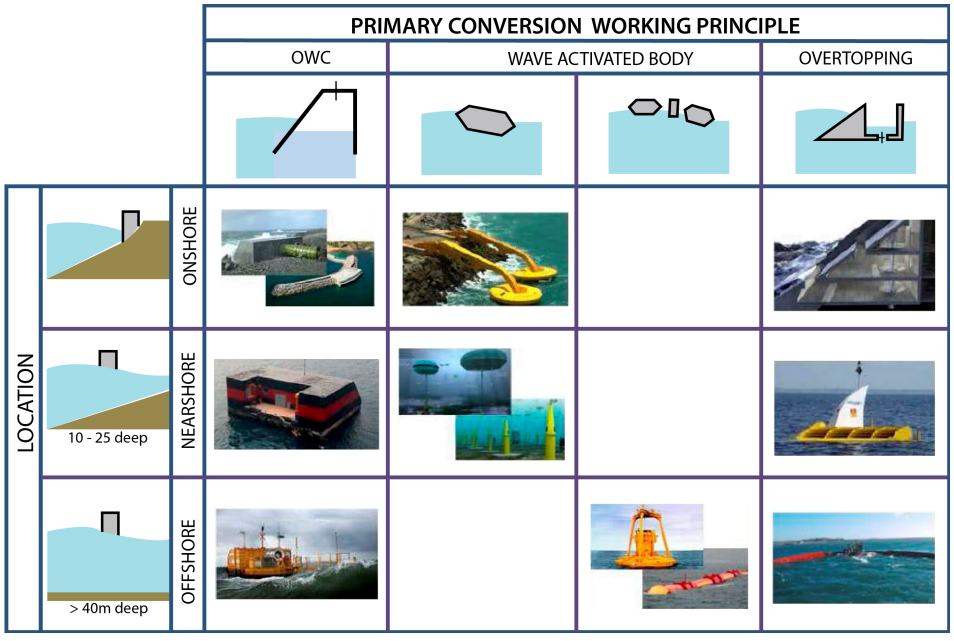

Figure 2-2.: Wave Energy Converters classification [26].

2.2.1. Types

Currently, the WECs can be classified into three predominant types, notwithstanding the considerable variation in designs and concepts, which are [21]:

- *Point absorber*: A point absorber has the main characteristic of possessing small dimensions in their mechanism compared to the incident wavelength. They absorb the energy from a floating structure that heaves up and down on the surface of the water, or due to pressure differential, the movements below the ocean surface. Because of their small size, wave direction is not essential for these devices. An example of point absorber is Ocean Power Technology's Powerbuoy, see Figure **2-3**.

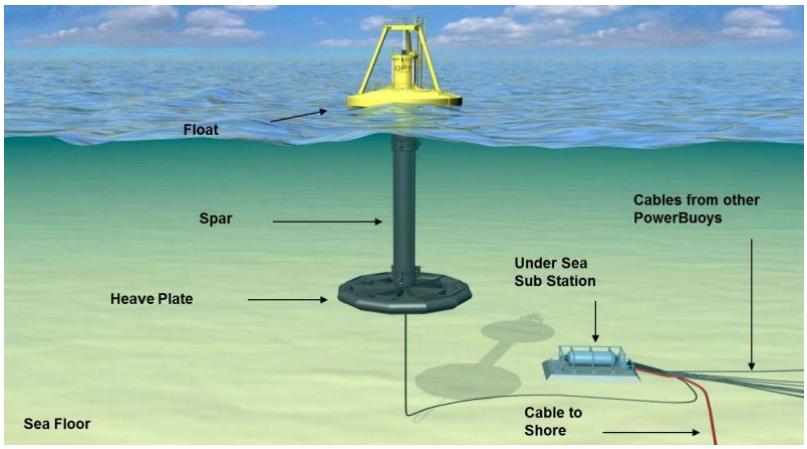

Figure 2-3.: Concept of the Powerbuoy WEC [27].

- *Attenuator*: The attenuators take advantage of their position in parallel with the swell to absorb the energy with which it comes, see Figure **2-4**. An example of an attenuator WEC is the Pelamis, developed by Ocean Power Delivery Ltd.

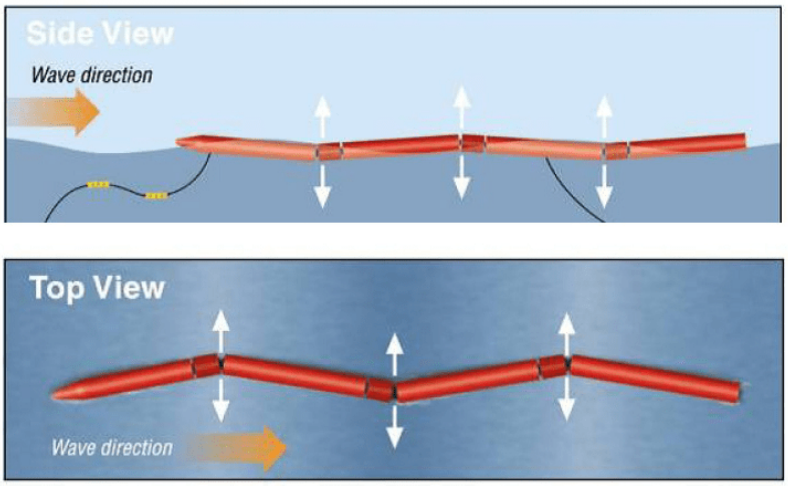

Figure 2-4.: Concept of the Pelamis [28].

- *Terminator*: Terminator devices focus their design in the principal axis parallel to the wavefront (perpendicular to the predominant wave direction) and physically intercept waves, see Figure **2-5**.

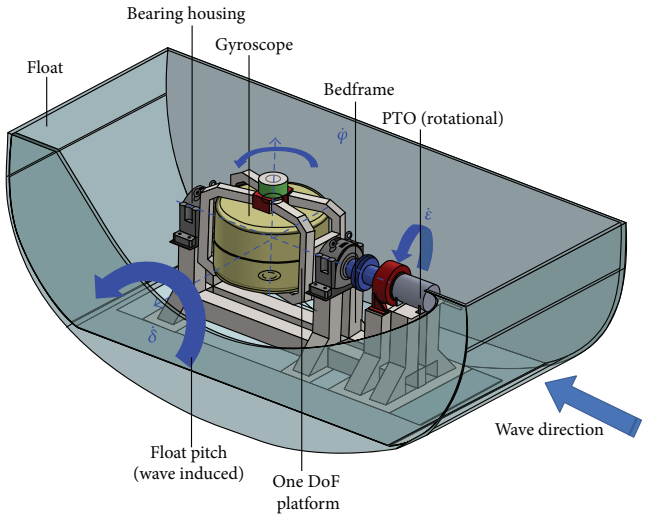

Figure 2-5.: Concept of the ISWEC [29]

2.2.2. Modes of operation

It is important to know that there is another other classification of devices by their mode of operation. Some significant examples are given below.

- **Submerged pressure differential**
  The submerged pressure differential device is composed of a submerged point absorber located under the ocean and uses the pressure difference above the converter between wave crests and troughs. It includes two main elements: a sea bed fixed air-filled cylin- drical chamber. As of the movement that the device has by the maximum amplitudes of the wave, it causes that water pressure that is above the converter compress the air inside the cylinder, which generating a displacement of the cylinder from top to bottom. As a trough passes over, the water pressure in the device begins to reduce and the upper cylinder rises.

  Now, among the main advantages that we find in this type of converter is its installation location, because it is completely submerged, which helps to avoids the impacts strong of the waves and in turn not generates a visual effect. However, the maintenance of this device is difficult, owing to a part of the converter seizing the sea bed like an anchor place. An example of this device is the Archimedes Wave Swing, see Figure **2-6**.

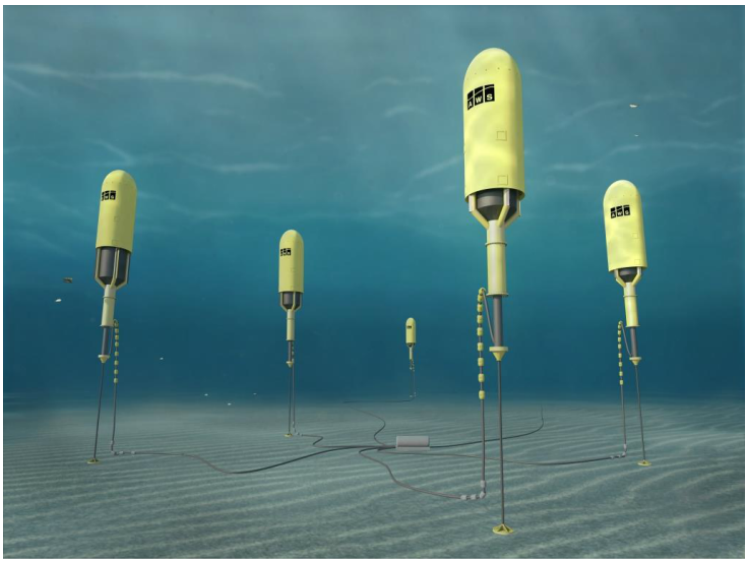

Figure 2-6.: Concept of the ARCHIMEDES WAVESWING [30].

- **Oscillating wave surge converter**
  An oscillating wave surge converter is a mechanism with a hinged deflector in perpendicular position respect to the direct wave, generating a back and forth movement in the converter. An example is the Aquamarine Power Oyster, a nearshore device, where the top of the deflector is above the water surface and anchored from the sea bed, see Figure **2-7**.

Figure 2-7.: Aquamarine Power Oyster system [31].

- **Oscillating Water Column (OWC)**
  The OWC is a converter characterized by having a chamber with an opening, located below the waterline. As the waves reach the device, the water generates pressure on the air inside the chamber. The displaced air reaches a Wells-type turbine and finally exits towards the atmosphere. This type of generator is entirely used in this kind of converter because the movement of the Blades is independent of the direction of the air flow. An example is the device Wavegen Limpet installed on Island Island, western Scotland, see Figure **2-8**.

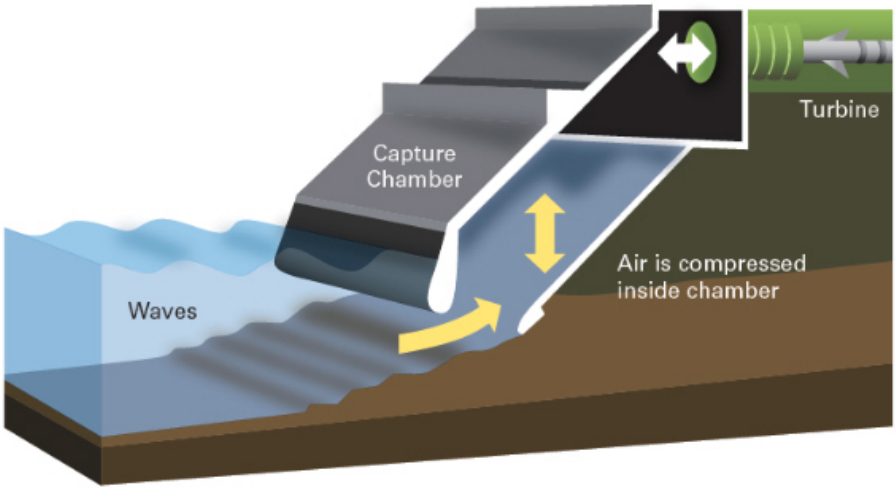

Figure 2-8.: Oscillating Water Column scheme [32].

- **Overtopping device** An Overtopping device takes advantage of the incidence of the waves to capture the water flow in a reservoir that is above sea level. When the deck is full it releases the water through the installed turbines. An example of this type of device is the Wave Dragon, see Figure **2-9**.

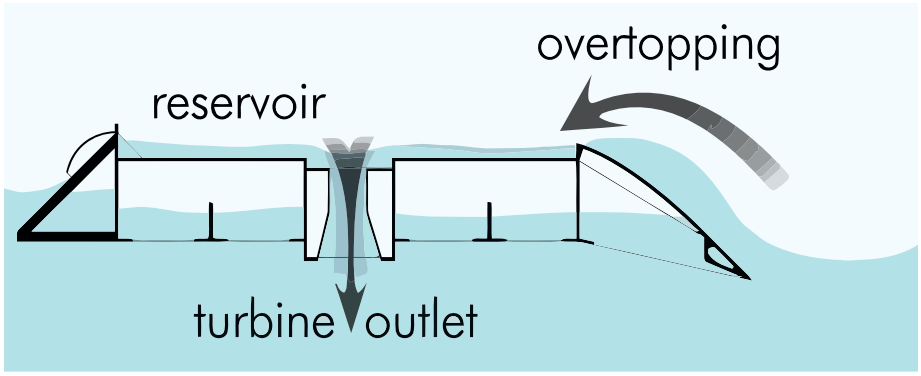

Figure 2-9.: Oscillating Water Column scheme [33].

2.3. Active Projects

Due to the extensive development of WECs, it will present brief insight into the current state of the wave energy industry with a selection of active WEC developers that have operational prototypes at sea.

- **AW-Energy**
  The Wave Roller concept consists of buoyant panels hinged at the sea bed, see Figure **2-10**. This converter operates in near-shore areas (approximately 0.3-2km from the shore) and depths between 8m and 20m. The capacity by one section is at between 350kW and 1000kW. The system has a hydraulic-based PTO, that converts the motion into electricity [34].

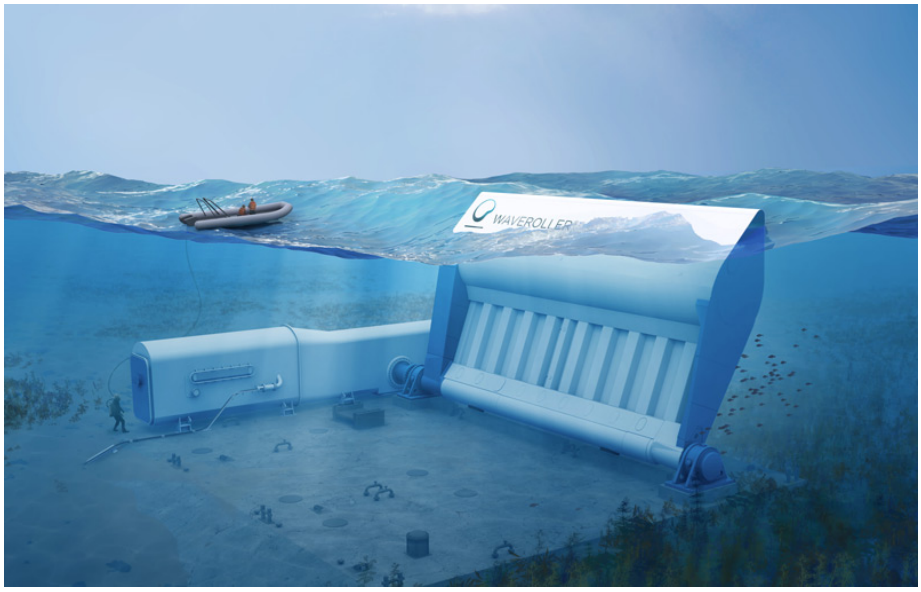

Figure 2-10.: WaveRoller project [34].

- **Wavestar**
  The Wavestar operates a 500kW test section in Hanstholm, Denmark. The main characteristic of this converter is multiple absorber systems. The operating principle consists in the absorption the power of wave utilizing the relative motion of absorbers and structure. The system has a hydraulic-based PTO, converting the motion into electricity, see Figure **2-11** [35].

Figure 2-11.: Wavestar project [35].

- **Aquamarine Power**
  This company deployed and tested two full-scale Oyster at EMEC: Oyster 1 with a capacity of 315kW of the capacity and Oyster 800 with 800kW at Orkney, Scotland. The design concept of this converter is a buoyant hinged flap attached to the seabed at around ten meters depth. This flap benefits by the wave movement for the wave, generating the drives of two hydraulic pistons which push high-pressure water to drive the conventional hydroelectric turbine, see Figure **2-12** [36].

Figure 2-12.: Oyster project [36].

- **Gibraltar Project**
  This company developed a first large-scale converter which is part of the Gibraltar project with a 100kW capacity; the total capacity of the power plant is 5MW in Gibraltar, United Kingdom. In operation mode, the floaters are going up

and down, pushing the hydro cylinders, which transmit hydraulic fluid through the pipes into the machinery room. The hydraulic fluid from the hydro cylinders is transferred into land-located accumulators. Inside the accumulators, a pressure has been created, which is used to turn the hydromotor, which turn the generator that sends clean electricity into the Gibraltar grid, see Figure **2-13** [37].

Figure 2-13.: Gibraltar project [37].

- **Ocean Power Technology**
  The PowerBouy consists of a float, spar, and heave plate. The float oscillates due to the motion of the waves. The spar maintains a relatively stationary position by the heave. When the buoy moves, this oscillating movement is converted to rotational movement, generating motion in the electrical generators that produce electricity that is exported for nearby marine applications through a submarine electrical cable. The range of power output is up to 3kW and up to 15kW, see Figure **2-14** [38].

Figure 2-14.: Powerbouy project [38].

- **Pelamis**
  This converter started with the installation and testing of four first version P1-machines, and are now operating two P2 prototypes of 750kW in Orkney, Scotland. The concept design consists of a moored articulated structure, with linked sections, moving with the motion of the waves. The power extraction is due to the joints from the relative movement of the parts, see Figure **2-15** [39].

Figure 2-15.: Pelamis project [39].

- **Seabased AB**
  The concept design consists of a floating buoy and linear generator, see Figure **2-16**. The oscillating movement of the buoy is due to interaction with the waves and transmit the energy through a steel line to a generator [40].

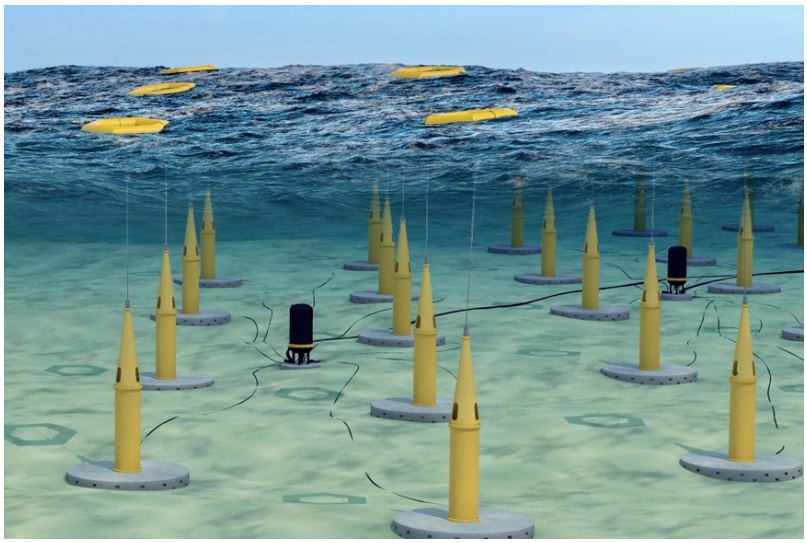

Figure 2-16.: Seabased project [40].

2.4. Prototypes of DMDS developed

According to Falcão [41], the development of mechanisms for Power taker-off (PTO) converters considers the essential aspects of harvesting power systems from the movement of ocean waves. For this reason, researchers have focused on designing different WECs, which have been built prototypes at scale to validate their operation, see Table **2-1**.

Reference	Development of a design methodology	WEC simulation	Type: Linear to rotary	Innovation	Tested/Scale
Pimienta, SanJuan, Oliveros, Gómez and Crisson	✓	✓	✓	Crank slider mechanism	✓
Sang, Karayaka, Yan and Zhang [42]	✗	✓	✓	Crank slider mechanism	✗
Agamloh, Wallace and von Jouanne [43]	✓	✓	✓	Contactless force transmission system/Ball screw nut mechanism	✓
Liang, Ai and Zuo [44]	✓	✓	✓	Rack and pinion motion rectifier	✓
De Koker, Degrieck, De Maeyer, Verbelen, Verbrugghe, Vantorre and Vandevelde [45]	✗	✓	✓	Planetary gear system with control transmission	✗
Boren, Lomonaco, Batten and Paasch [46]	✓	✓	✓	Vertical axis pendulum	✓
Takaramoto, Kashiwagi and Sakai [47]	✗	✓	✓	Winging mass like a pendulum	✗
Dai, Chen and Xie [48]	✗	✓	✓	Pulley/spring connected to two submerged bodies	✓
Hadano, Lee and Moon [49]	✗	✓	✓	Closed loop with 4 pulleys	✓
Kim, Wata, Zullah, Ahmed and Lee [50]	✓	✓	✓	A working fluid inside the buoy operates a turbine	✓

Table 2-1.: Converters PTOs developed.

Therefore, the continuous technological development has led to the search for different mechanisms of low cost and simplicity in its design, intending to generate competitiveness in the commercial stage, as in the case of Sang et al. [42]. The mechanism proposed is a slider-crank system being a mechanism used in conventional combustion engines, where their study focus have been the simulation of control systems that help maximum energy extraction of the converter [51, 52, 53]. For this reason, in search of strengthening the research carried out, the study of this thesis focuses on proposing a methodology for the design of this type of WEC and validate it with the construction of a prototype at scale, which has not been the object of study.

3. Modelling of Slider-Crank WEC

This chapter discusses the theoretical background needed to understand the modeling of ocean waves and WEC. The chapter has four parts, covering: Overall System Model , the basic properties of ocean waves, the hydrodynamics model, the kinematical model and the application of the virtual work and D' Alembert analysis in the WEC mechanism.

3.1. Overall System Model

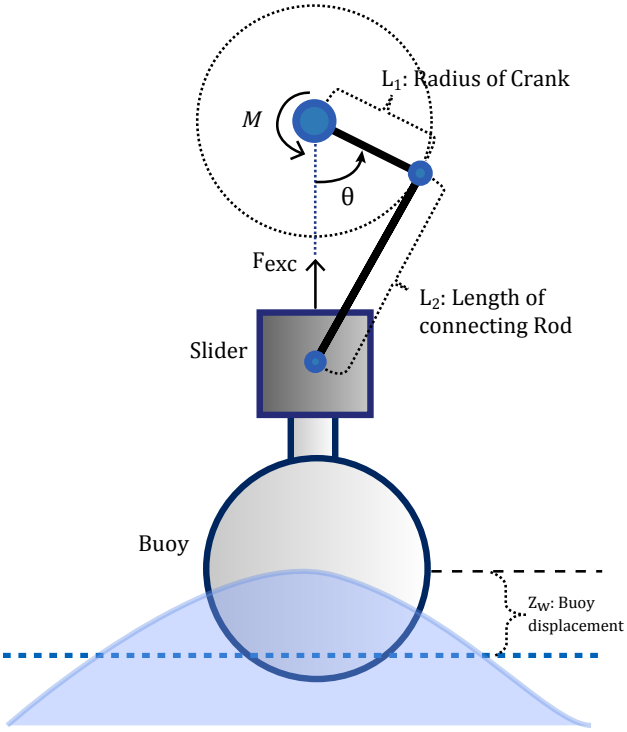

Figure 3-1.: Slider-Crank System [42].

The proposed design for the WEC is inspired by the system used in the internal combustion engine of a single cylinder. The mechanism presented is formed by a piston, a connecting rod, a crank, and a buoy, where the buoy is the only who is not used in the internal combustion engines. The operation of the device is given as follows: The piston is attached to the WEC in such a way as to follow the orientation of the waves movement. Starting from the force exerted by the waves on the buoy, the connecting rod is displaced from its resting state, causing the rotational movement of the crank at the end of the converter. This transmitted energy generates a torque at the exit of the mechanism, which is necessary for the rotation in the input shaft of the electric generator. In Figure **3-1**, the physical model of the mechanism is exposed with the variables to be considered in our analysis.

3.2. Ocean Waves

The most elemental waveform is a two-dimensional wave of a harmonic. However, the waves in the sea have variability in their height and wavelength, which makes this phenomenon is random and non-deterministic. By such characteristics, it is impossible to determine the variation of the surface before it occurs, so it is necessary to have a stochastic model to describe it.

Waves can be divided into two groups: regular and irregular. Regular waves are the one in which the waves move in a single direction following a sinusoidal shape of a harmonic. On the other hand, an irregular swell can be seen as a combination or overlap of a large number of regular sine wave components with different frequencies, heights and directions. The analyses will be carried out with regular waves because they provide a sufficiently realistic scenario for this object of study [54]. To delve deeper into the irregular waves topic is available in Appendix A.

3.2.1. Regular Wave Theory

The wave motion of this type may have a sinusoidal form, long-crested and progressive. The mains characteristics of this motion type are that the wave repeats itself and has a smooth shape. The basic parameters used to describe the ocean wave are presented in the next Figure **3-2**:

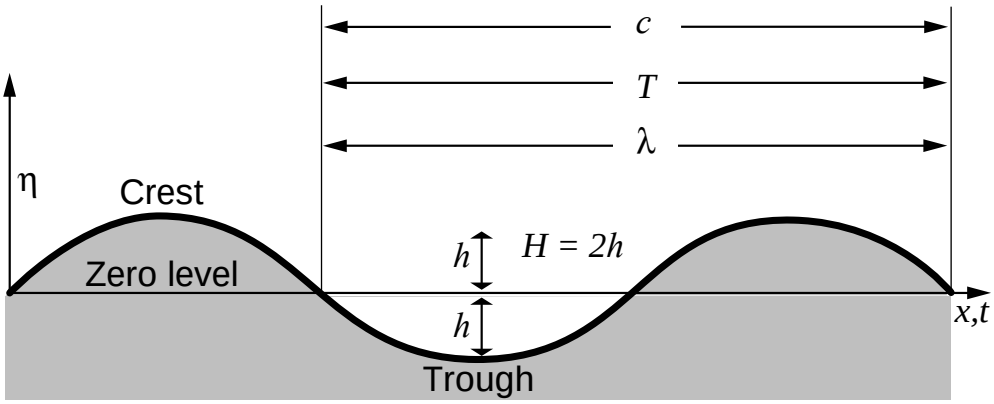

Figure 3-2.: Classification of ocean waves by period and by source [54].

- *Amplitude h:* The Maximum displacement from mean sea level (in meters).
- *Frequency f:* The number of crests which pass a fixed point in one second. It is measured in Hertz and it is equal to $1/T$.
- *Period T:* Time interval (in seconds) between two successive crests.
- *Phase Speed c:* Speed at which the wave profile travels. The speed at which the trough and crest of the wave advance, equal to λ/T, is commonly defined as *wave speed*.
- *Wavelenght λ:* Horizontal distance between two consecutive crests (in meters).
- *Wave Height H:* It is the Difference in surface elevation between the wave crest and the previous wave trough, equal to $2h$.

The presented simple wave profile has the form of a sinusoidal wave, see Equation 3-1,

$$Z(x,t) = h\sin(kx - wt) \tag{3-1}$$

where $k = 2\pi/\lambda$ is the *wavenumber* and $w = 2\pi/T$ is the *angular frequency*.

3.3. Stability Model

In WECs, analyses begin with the study of the hydrodynamic model. Hydrodynamic theory studies the movement and forces that interact on fixed and floating bodies

located on a moving fluid [14]. To conduct the hydrodynamic analysis of this WEC, a spherical semi-submerged buoy is used and assumed infinite water depth to conserve the linearity assumption so that we can use the differential Equation 3-2 [55] that describes the buoy motion based on hydrodynamic forces acting on it,

$$(m_a + m_b)\ddot{z} + B\dot{z} + Cz = F_{exc} + F_r \tag{3-2}$$

where z is the buoy center of gravity displacement with respect to the water surface without disturbance, $\dot{z}$ the buoy velocity, m_a is the semi-submerged buoy mass, m_b is the buoy mass, B is the total damping coefficient, C is buoy hydrostatic stiffness, F_{exc} is the heave excitation force and F_r is radiation force.

The total mass of spherical buoy of radius a is given by the next equations,

$$m_b = \rho_b \frac{4\pi}{3} a^3 \tag{3-3}$$

$$m_a = \rho_w \frac{2\pi}{3} a^3 \tag{3-4}$$

where ρ_b and ρ_w are the buoy density and the sea water density, respectively.

For the second term of the Equation 3-2, $B\dot{z}$ is related with the damping force, represented as F_d. In this case, this force only depends on the submerged volume of the buoy and not by the buoy velocity [56]. It is represented by the following equation,

$$F_d = m_a \omega \{B^{(0)} \cos \omega t - A^{(0)} \sin \omega t\} \tag{3-5}$$

where ω is the wave angular velocity, $B^{(0)}$ and $A^{(0)}$ are the non-dimensional added mass and damping coefficient associated with the heaving motion of the body. These coefficients are calculated considering the product between wave number k and radio buoy [56]. Also, for infinite wave depth, k can be calculated as [42],

$$k = \frac{\omega^2}{g} \tag{3-6}$$

where g is the gravity.

Now, Cz is the buoyancy hydrostatic force, represented as F_b, depends on the differential between the displacement of buoy position with the wave amplitude and can

be given by,

$$F_b = \rho_w g \pi a^2 z \tag{3-7}$$

In Equation (3-2), F_r can be calculated as [55],

$$F_r = -R_{rad}\dot{z} \tag{3-8}$$

where R is the radiation coefficient and is equally to [42],

$$R_{rad} = R_v + R_f + \varepsilon_r(ka)\omega m_a \tag{3-9}$$

where R_v is the viscous force coefficient, R_f is the friction force coefficient and $\varepsilon_r(ka)$ is radiation resistance coefficient. The $\varepsilon_r(ka)$ is calculated as suggests in literature [56].

Finally, for simplicity in our study, the sinusoidal regular waves were considered. Therefore, the shape of the wave is expressed by the following equation,

$$z_w = h \cdot sin(wt) \tag{3-10}$$

where h is the amplitude of the wave.

3.4. Kinematical Analysis

The closed-loop diagram of the mechanism is presented in Figure **3-3**. For simplification of the analysis, the origin O of the system is considered at the centre of the wave. The variable L_1 represents the radius of the crank, while L_2 is the length of the connecting rod that assembles the buoy with the crank. The angle θ_1 describes the angular rotation of the crank, while the angle θ_2 describes the rotation of the connecting rod. The variable L_3 represents the distance between O and the centre of the crank. The vector $\vec{q}$ represents the vertical displacement of the buoy with respect to O, and is given by the following equation:

$$\vec{q} = \begin{bmatrix} 0 \\ h\sin(\omega t) \end{bmatrix} \tag{3-11}$$

Where ω and h are the angular frequency and amplitude of the waves, respectively; and t is the time.

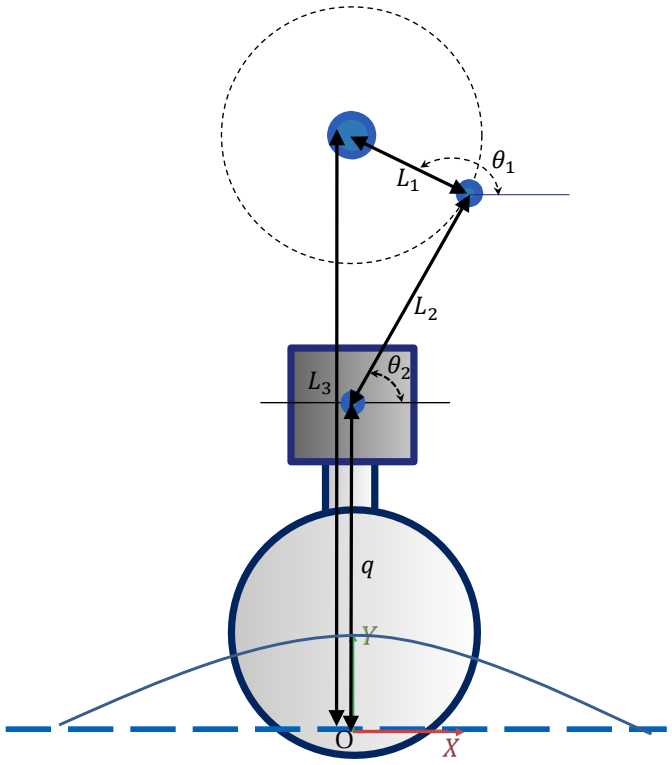

Figure 3-3.: kinematic diagram of the slider-crank System [42].

Thus, the closed-loop equation of the system is given as follows:

$$\begin{bmatrix} 0 \\ q \end{bmatrix} + L_1 \begin{bmatrix} \cos\theta_1 \\ \sin\theta_1 \end{bmatrix} + L_2 \begin{bmatrix} \cos\theta_2 \\ \sin\theta_2 \end{bmatrix} = \begin{bmatrix} 0 \\ L_3 \end{bmatrix} \tag{3-12}$$

Then, solving Equation 3-12, using the method of Tangent half-angle substitution [57], yields the following equation for the angle θ_2:

$$\theta_2 = 2\arctan\left(\frac{-C_2 \pm \sqrt{C_2^2 - 4C_1C_3}}{2C_1}\right) \tag{3-13}$$

the terms c_i are a function of the dimensions of the WEC, and are expressed as follows,

$$C_1 = q^2 - 2L_3q - L_1^2 + L_2^2 + L_3^3 \tag{3-14}$$

$$C_2 = 4L_2q - 4L_2L_3 \tag{3-15}$$

$$C_3 = q^2 - 2L_3q - L_1^2 + L_2^2 + L_3^2 \tag{3-16}$$

Then, the result of θ_2 is plugged into Equation 3-13 to obtain the solution of θ_1, as follows:

$$\theta_1 = \arccos\left(-\frac{L_2}{L_1} * \cos\theta_2\right) \tag{3-17}$$

3.4.1. Velocity and acceleration analysis

Once is determined the position analysis of the WEC, the following step is to obtain the relation of the velocity of each link related to the velocity of the buoy. Thus, deriving Equation 3-12, and grouping the result in a matrix form, the following relation holds:

$$\begin{bmatrix} -L_1\sin\theta_1 & -L_2\sin\theta_2 \\ L_1\cos\theta_1 & L_2\cos\theta_2 \end{bmatrix} \begin{bmatrix} \dot{\theta}_1 \\ \dot{\theta}_2 \end{bmatrix} = \begin{bmatrix} 0 \\ -\dot{q}_1 \end{bmatrix} \tag{3-18}$$

Where the terms $\dot{\theta}_1$ and $\dot{\theta}_2$ represent the angular velocity of the crank and the connecting rod, respectively. The variable $\dot{q}$ is obtaining by deriving y term of equation 3-11; the result is presented below:

$$\dot{q} = \omega h\cos\omega t \tag{3-19}$$

Analogously, the relation of the accelerations of the system is obtained by the derivation of Equation 3-18. Thus, regrouping the resulting equation in matrix form, the following equation holds:

$$\begin{bmatrix} -L_1\sin\theta_1 & -L_2\sin\theta_2 \\ L_1\cos\theta_1 & L_2\cos\theta_2 \end{bmatrix} \begin{bmatrix} \ddot{\theta}_1 \\ \ddot{\theta}_2 \end{bmatrix} = \begin{bmatrix} L_1\dot{\theta_1}^2\cos\theta_1 + L_2\dot{\theta_2}^2\cos\theta_2 \\ -L_1\dot{\theta_1}^2\sin\theta_1 - L_2\dot{\theta_2}^2\sin\theta_2 - \ddot{q}_1 \end{bmatrix} \tag{3-20}$$

Note that the term $\ddot{q}$ corresponds to the derivative of Equation 3-19, as presented

below:

$$\ddot{q} = -\omega^2 h \sin wt \tag{3-21}$$

3.5. Virtual Work Principle

The virtual work formulation is developed for the force analysis of the WEC. This principle consider the system in static equilibrium, due to the D' Alembert's principle, which states the inertial forces acting upon the system can be regarded as an external force as presented below,

$$\sum \overline{f}_{ext} = \sum f_{ext} - ma_c = 0 \tag{3-22}$$

$$\sum \overline{n}_{ext} = \sum n_{ext} - I_c\omega = 0 \tag{3-23}$$

Where $\sum \overline{f}_{ext}$ and $\sum \overline{n}_{ext}$ are the total forces and moments acting on the body, including the inertial forces, while $\sum f_{ext}$ and $\sum n_{ext}$ are the external forces acting upon the body; m is the mass of the body, a_c is the acceleration of the mass centre and I_c is the inertia of the gravity centre of the body. Thus, considering a virtual displacement of $\delta(.)$ for each rigid body constituting the mechanism, the following equation holds:

$$\delta W = \sum \bar{\mathcal{F}} \cdot \delta \mathcal{X}_i = 0 \tag{3-24}$$

Where δW is the virtual work done by the mechanism; $\mathcal{F}$ is a vector that includes the external forces and torques of each component of the mechanism, this vector is usually known as the wrench. This vector is expressed in the following vector:

$$\sum \bar{\mathcal{F}} = \begin{bmatrix} \sum \bar{f}_{ext} \\ \sum {}^{c}\bar{n}_{ext} \end{bmatrix} \tag{3-25}$$

Note that the reaction forces between components banish due to the work done for these forces is equal to zero [58]. Thus, the term $\bar{\mathcal{F}}$ is reduced to the forces produced by the inertia of the element, and the input/output forces, in other words, the forces that realize work. Then, Equation 3-24 is rewritten in terms of the components that

compose the WEC as follows:

$$\delta W = \begin{bmatrix} 0 & \tau + \bar{\mathcal{F}}_{buoy} & 0 \end{bmatrix} \begin{bmatrix} 0 \\ \delta q \\ 0 \end{bmatrix} - \mathcal{M}\delta\theta_1 + \bar{\mathcal{F}}_1^T \begin{bmatrix} 0 \\ 0 \\ \delta\theta_1 \end{bmatrix} + \bar{\mathcal{F}}_2^T \begin{bmatrix} \delta x_{cg2} \\ \delta y_{cg2} \\ \delta\theta_2 \end{bmatrix} = 0 \tag{3-26}$$

Where the term τ represents the external force that exerts the waves on the buoy, this force is regarded as the input of the system; The term $\bar{\mathcal{F}}_{buoy}$ represents the wrench of the buoy, which is expressed in the following equation:

$$\bar{\mathcal{F}}_{buoy} = \begin{bmatrix} 0 \\ -m_{buoy}\ddot{q} \\ 0 \end{bmatrix} \tag{3-27}$$

Where m_{buoy} is the mass of the buoy.

The term $\mathcal{M}$ represent the external moment produced by a theoretical electrical generator; the term $\bar{\mathcal{F}}_1$ is the wrench of the crank, which is given by the following equation:

$$\bar{\mathcal{F}}_1 = \begin{bmatrix} 0 \\ 0 \\ -I_{cg1}\ddot{\theta}_1 \end{bmatrix} \tag{3-28}$$

Where the term I_{cg1} is the inertia in the center of gravity of the crank.

Note that the term corresponding to sum of forces in Equation 3-28 is zero, due to it is considered that the inertia of the crank is attached to a flywheel that moves the center of mass of the crank to the pivot.
Lastly, the term $\bar{\mathcal{F}}_2$ is expressed below:

$$\bar{\mathcal{F}}_2 = \begin{bmatrix} -m_2 * \vec{a}_{cg2} \\ -I_{cg_2}\ddot{\theta}_2 \end{bmatrix} \tag{3-29}$$

The term $\vec{a}_{cg2}$ is expressed using the results from Equation 3-20 as follows:

$$\vec{a}_{cg2} = L_{cg} \begin{bmatrix} -\ddot{\theta}_2 \sin(\theta_2 + \alpha) - \dot{\theta_2}^2 \cos(\theta_2 + \alpha) \\ \ddot{\theta}_2 \cos(\theta_2 + \alpha) - \dot{\theta_2}^2 \sin(\theta_2 + \alpha) \end{bmatrix} \tag{3-30}$$

The term L_{cg2} refers to the distance between the buoy to the centre of gravity of the connecting rod; While the variable α refers to the angle that is formed between the centre of gravity, the assembly point of the connecting rod with the buoy, and the assembly point of the connecting rod with the crank.

Thus, once the inertial parameters conforming Equation 3-26 are established, the following step is to express each of the differential displacement terms as a function of the differential displacement of the buoy to simplify Equation 3-26 into the dynamical equation of the WEC. In the following, each differential term is presented individually.

3.5.1. Differential rotations

The differential rotations $\delta\theta_1$ & θ_2 are treated simultaneously. However, to solve then it is required to acknowledge the following property of the differential displacement [59]:

$$\frac{\delta\dot{r}}{\delta\dot{q}} = \frac{\delta r}{\delta q} \tag{3-31}$$

Thus, Equation 3-31 permits the utilization of Equation 3-18 to calculate the differential displacements $\delta\theta_1$ & θ_2, obtaining:

$$\delta\theta_1 = \frac{\delta q}{L_1} \frac{\tan\theta_2}{\sin\theta_2 - \cos\theta_2 \tan\theta_1} \tag{3-32}$$

$$\delta\theta_2 = \frac{\delta q}{L_2} \frac{\tan\theta_1}{\sin\theta_2 - \cos\theta_2 \tan\theta_1} \tag{3-33}$$

3.5.2. Differential displacement of the coupling rod

The differential displacement of the centre of gravity of the coupling link is obtained by expressing the velocity of the centre of gravity as follows:

$$\begin{bmatrix} \dot{x}_{cg2} \\ \dot{y}_{cg2} \end{bmatrix} = \begin{bmatrix} 0 \\ \dot{q} \end{bmatrix} + L_{cg} \begin{bmatrix} -\dot{\theta}_2 \sin(\theta_2 - \alpha) \\ \dot{\theta}_2 \cos(\theta_2 - \alpha) \end{bmatrix} \tag{3-34}$$

Then, recurring to Equation 3-31, and replacing Equations 3-32 & 3-33 into 3-34 yields:

$$\begin{bmatrix} \delta x_{cg2} \\ \delta y_{cg2} \end{bmatrix} = \begin{bmatrix} 0 \\ \delta q \end{bmatrix} + L_{cg} \begin{bmatrix} -\frac{\delta q}{L_2} \frac{\tan\theta_1}{\sin\theta_2 - \cos\theta_2 \tan\theta_1} \sin(\theta_2 - \alpha) \\ \frac{\delta q}{L_2} \frac{\tan\theta_1}{\sin\theta_2 - \cos\theta_2 \tan\theta_1} \cos(\theta_2 - \alpha) \end{bmatrix} \tag{3-35}$$

Thus, replacing Equations 3-27, 3-28, 3-29, 3-30, 3-32, 3-33, and 3-35 into Equation 3-26 yields the dynamical model of the system.

4. Methodology of design of the WEC

In the following a methodology of the design of the WEC is established. This methodology uses the results of the dynamical model to establish the dimension of the WEC that produces a continuous motion of the crank. The methodology is presented in Figure **4-1**. The explanation of each step is presented in the following.

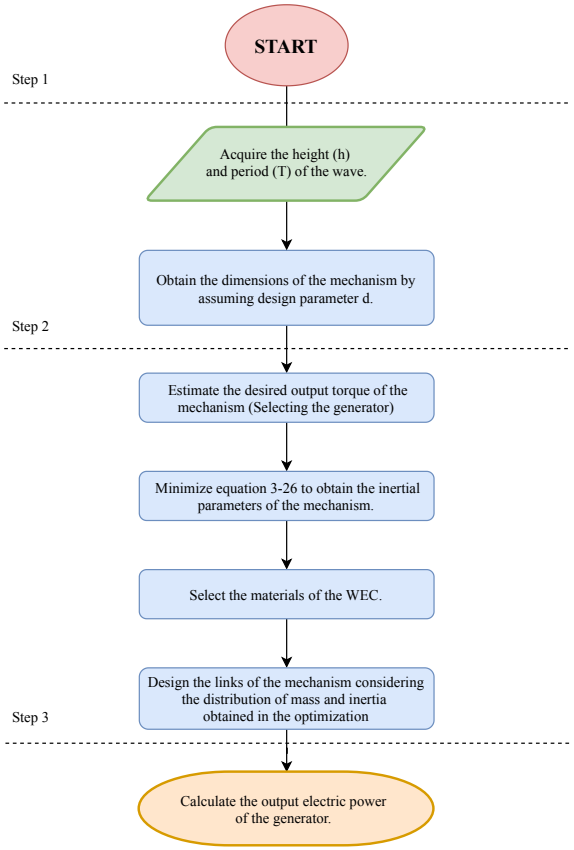

Figure 4-1.: Flowchart of the methodology for the WEC design.

4.1. Dimensioning of the Crank and Connecting rod

The dimensions of the mechanism are selected as a function of the wave period and amplitude, to guarantee the rotational movement of the crank. Figure **4-2** presents the two limit positions of the crank relative to the wave. The following equations present the conditions for the wave maximum and minimum levels, respectively.

$$L_1 - L_2 = d - h + a \tag{4-1}$$

$$L_2 + L_1 = d + h - a \tag{4-2}$$

Where the term d is a design variable that permits to position the mechanism relative to the wave and a is the radius of the buoy. Then, solving the system of equation, the following relation holds:

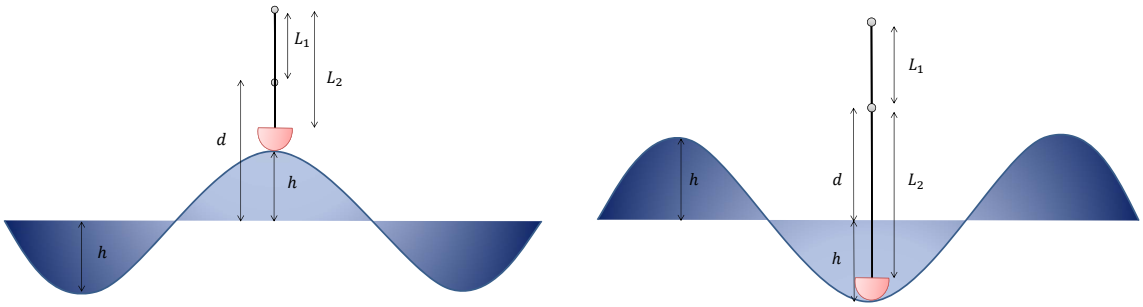

(a) The buoy in the minimum level of the wave.

(b) The buoy in the maximum level of the wave.

Figure 4-2.: Limit positions of the crank relative to the wave.

$$L_1 = h \qquad L_2 = d - a \tag{4-3}$$

4.2. Optimal inertial parameters of the links of the mechanism

Once the kinematical dimensions of the mechanism are obtained, the following step is to define the inertial properties of each of the mechanism links. This is achieved by recurring to the optimization of Equation 3-26. The process of optimization seeks to stablish the inertial parameters that maintains a constant output torque $\mathcal{M}$, while

minimizing the input force τ. Thus, calculating the values of τ along a cycle of the mechanism, the objective function became the mean of τ as follows:

$$\tau_{mean} = \frac{1}{T}\int_0^T \tau dt \tag{4-4}$$

Equation 4-4 is subject to the following restrictions:
Mass of the crank

$$M_{1-min} < m_1 < M_{1-max} \tag{4-5}$$

Mass of the connecting rod

$$M_{2-min} < m_2 < M_{2-max} \tag{4-6}$$

Inertia of the crank

$$I_{1-min} < I_1 < I_{1-max} \tag{4-7}$$

Inertia of the connecting rod

$$I_{2-min} < I_2 < I_{2-max} \tag{4-8}$$

Where M_{1-min}, is the minimum mass of the crank; M_{1-max},is the maximum mass of the crank; M_{2-min}, is the minimum mass of the connecting rod;M_{2-max}, is the maximum mass of the connecting rod; I_{1-min}, is the minimum inertia of the crank; I_{1-max}, maximum inertia of the crank; I_{2-min}, is the minimum inertia of the connecting rod; and I_{2-max}, is the maximum inertia of the connecting rod.

Note that the inertia of each link depends also of the selection of $\mathcal{M}$. The higher the values of $\mathcal{M}$ would require to take in consideration the internal forces of the mechanism, due to the system may fail due to the high stress produced by the high torque. Thus, the values of inertia and mass should be selected accordingly to the requirements of resistance of materials.

4.3. Power output of the electric generator

In wave energy generation systems, it is essential to keep in mind the variable and unpredictable nature of the wave behaviour for the selection of the electric generator

in the WECs, due to a rectification stage is necessary for the voltage signal produced in the generator terminals to maintain the frequency of the supply voltage wave in the load constant.

The use of AC generator presents random frequencies in the voltage waves produced by the WEC movement, which leads to the design of a rectifying circuit to transform it into DC to be in turn stored in batteries. After accumulating this energy, it would subsequently lead to the use of an inverter circuit to obtain an AC signal with the desired magnitude and frequency. Unlike a DC generator, it could connect directly to a battery, which would prevent a rectifier circuit, followed by the inverter circuit mentioned above. According to the above, in this master's thesis Permanent Magnet DC (PMDC) generator will be used. The storage stage named above is not considered at the design stage due to the scope of this project, which implies intermittent power generation in terminals.

4.3.1. PMDC: Operation mode and Electric Design

Operation mode

The PMDC is composed for a stator and rotor, see Figure **4-3**. The stator is the fixed section of the motor where the rotor rotates, which is made by a pair of permanent magnets aligned, with the objective that poles of opposite polarities face each other. Thus, a magnet has two polarities, north and south, located near the armor. Therefore, the magnetic field flow flows from one permanent magnet to another through the metal armature [60].

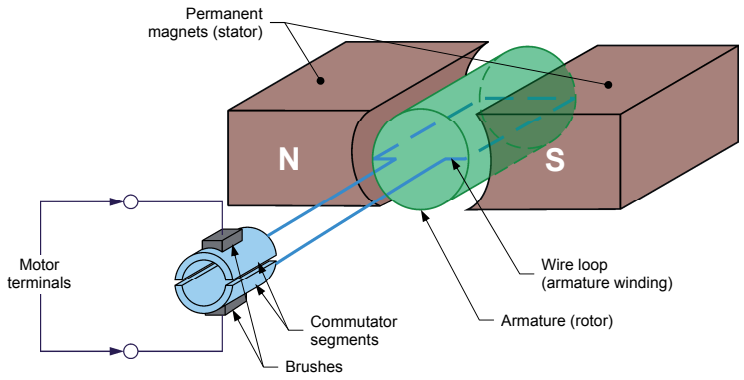

Figure 4-3.: Parts of PMDC [61].

On the rotor side, this is the rotating part of the motor, which is made of a wire loop mounted on a rotating metal armature. Each end of the loops is connected to the motor stator terminals using a commutator and a pair of brushes [60].
Now, the operating of the motor as a generator is given from the rotational motion of the rotor within a magnetic field generated by the stator's permanent magnets. The magnetic flux ϕ that passes through the loop varies, E_1, creating a voltage at the terminals. The voltage E_1 is taken by the two sections of the switch and delivered to the brushes ($B+$ and $B-$), which are connected to the motor terminals, see Figure **4-4**.

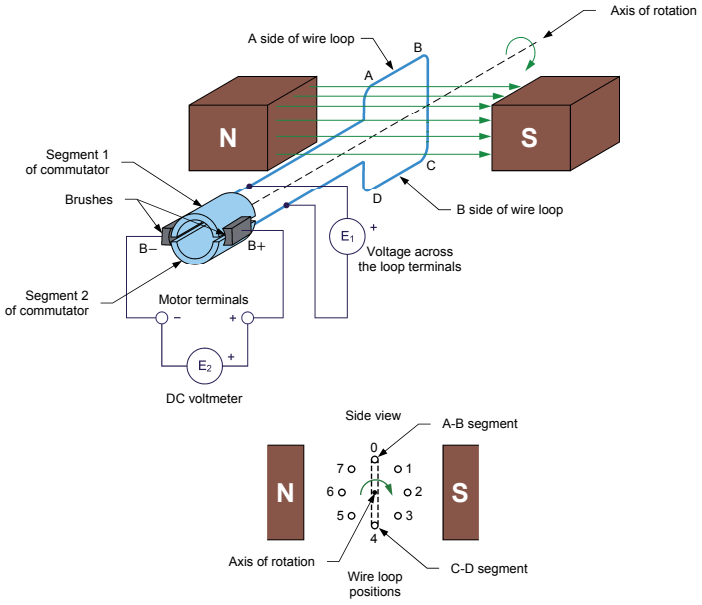

Figure 4-4.: PMDC operating as a generator [61].

Electric Design

The equivalent circuit of a PMDC can be represented in Figure **4-5** [62],

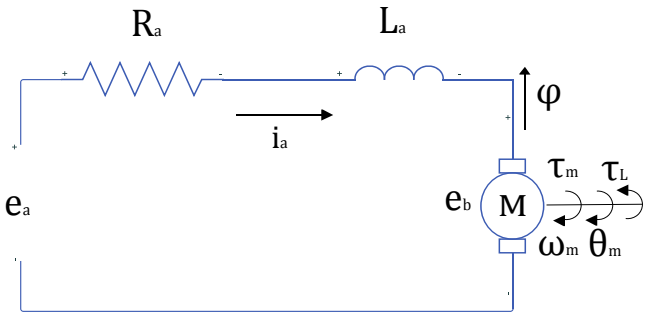

Figure 4-5.: Equivalent circuit of a PMDC [62].

where e_a is the voltage generated, the variable R_a represent the armature resistance; the L_a represent the armature inductance of the motor; the variable e_b represents the Counter-electromotive force; i_a represent the armature current; ϕ is magnetic field in iron core; τ_L is the load torque; τ_m is the torque from the electric motor; ω_m is the angular speed of the rotor and θ_m describe the angular displacement of the motor.

The flow in the iron is defined as constant when permanent magnets generate it, and it is defined as:

$$\tau_m = K_t i_a \tag{4-9}$$

where K_t is the constant torque or mechanical constant.
On the other hand, it can be established that there is a linear proportional relationship between the voltage generation in the motor e_b, which represents the back electromotive force present in the armature, and the perceived velocity in the rotor axis. Thus, it is defined that:

$$e_b = K_e \omega \tag{4-10}$$

where K_e is the angular velocity of the rotor. According to the above, a voltage analysis is performed in the loop of the equivalent circuit, shown below,

$$e_a - V_R - V_L + e_b = 0 \tag{4-11}$$

$$e_a - R_a i_a - L_a \frac{di_a}{dt} + K_e \omega = 0 \tag{4-12}$$

Considering that it is a circuit in direct current, the current is constant in time and therefore, it would have to,

$$ea - R_a i_a - K_e \omega = 0 \tag{4-13}$$

Dc generator and WEC

Now, according to Figure **4-5**, the equivalent circuit of the PMDC connected to the WEC can be represented as,

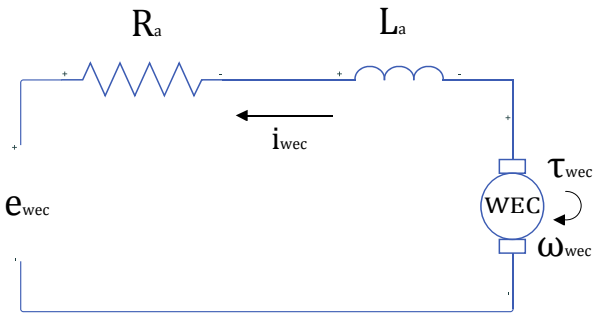

Figure 4-6.: Equivalent circuit of a PMDC connected to the WEC.

where τ_{wec} is the torque from the WEC and ω_{wec} is the angular velocity of the WEC.

The τ_{wec} is expressed using the results from Equation 3-28 as follows:

$$\tau_{wec} = \mathcal{F}_1 L_1 = I_{cg1} \ddot{\theta}_1 L_1 \tag{4-14}$$

Then, recurring to Equation 4-9, and replacing into Equation 4-14, the armature current is expressed in the following equation:

$$i_{wec} = \frac{I_{cg1} \ddot{\theta}_1 L_1}{k_t} \tag{4-15}$$

Thus, Equation 4-13 permits the utilization of Equation 4-15 to calculate the output

voltage of the DC generator:

$$e_{wec} = R_a \frac{I_{cg1}\ddot{\theta}_1 L_1}{k_t} + K_e \omega_{wec} \tag{4-16}$$

Finally, the output electric power of the generator, P_G, and the electric power in the load, P_{Load} are defined as,

$$P_G = e_{wec} \cdot i_{wec} = \left(\frac{R_a I_{cg1}\ddot{\theta}_1 L_1}{k_t} + K_e \omega_{wec} \right) \cdot \frac{I_{cg1}\ddot{\theta}_1 L_1}{k_t} \tag{4-17}$$

$$P_{Load} = \frac{e_{wec}^2}{R_{Load}} = \frac{\left(\frac{R_a I_{cg1}\ddot{\theta}_1 L_1}{k_t} + K_e \omega_{wec} \right)^2}{R_{Load}} \tag{4-18}$$

5. Results and Experimentation

In the following, the implementation of the methodology is evaluated on a laboratory scale. Thus, this section presents the equipment used to conduct the experimentation and the results obtained.

5.1. Case study

The detailed statistics of the waves are generated in a scaled wave tank build in the Universidad del Norte, which serves as a study case for the construction of the WEC based on the methodology previously developed. The system designed and built for wave generation is a four-bar mechanism, where the dimensions were according to the working space of the wave tank. The combinations of wave period and wave height used in the experiment are: 10 s/0.015 m, 11 s/0.015 m and 12 s/0.015m; and the resistance used in the experiment are: 5.7Ω, 7.8Ω and 12.5Ω.

5.1.1. Wave Generator

A wave generator was made to establish the condition of the ocean on a laboratory scale, as presented in Figure **5-1**. The dimensions of the tank are presented in Table **5-1**. The mechanism proposed to guarantee the wave generation correct is a four-bar mechanism, which is shown as Figure **5-2**. The wave generator uses a stepper motor DC of reference NEMA 23 for the rotational movement in the input, where a microcontroller Arduino One controls its velocity and torque. The rotational movement is converted to an oscillatory movement, due to the action of the four-bar mechanism. Thanks to the action of the wavemaker, the waves are obtained. Then, the period and height of the waves were obtained using a recording of the displacement and using the software Kinovea to process the images of the video. The results of the procedure are presented in Figure **5-3**. Note the depth of water for this analysis was 24 cm, as presented in Figure **5-1**. Furthermore, within the tank is installed a structure to simulates a beach to avoid the reflection of the waves.

Variable	Dimension (cm)
Width	26.1
Length	145
Depth	30

Table 5-1.: Tank dimensions

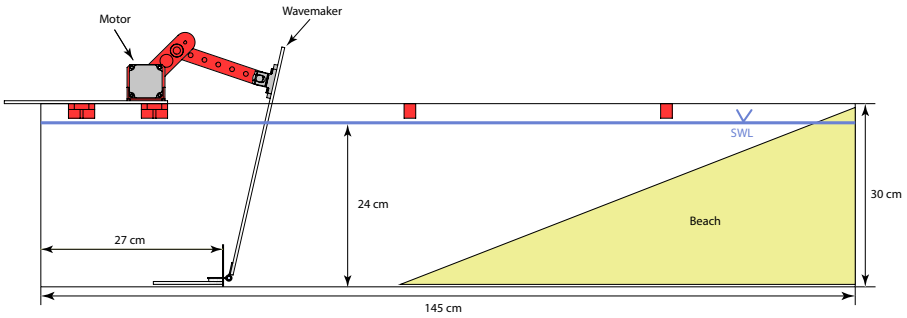

Figure 5-1.: Wave tank layout and dimensions.

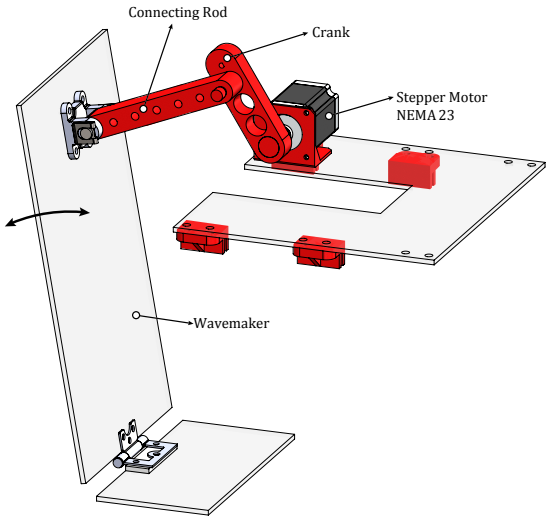

Figure 5-2.: Wave Generator mechanism.

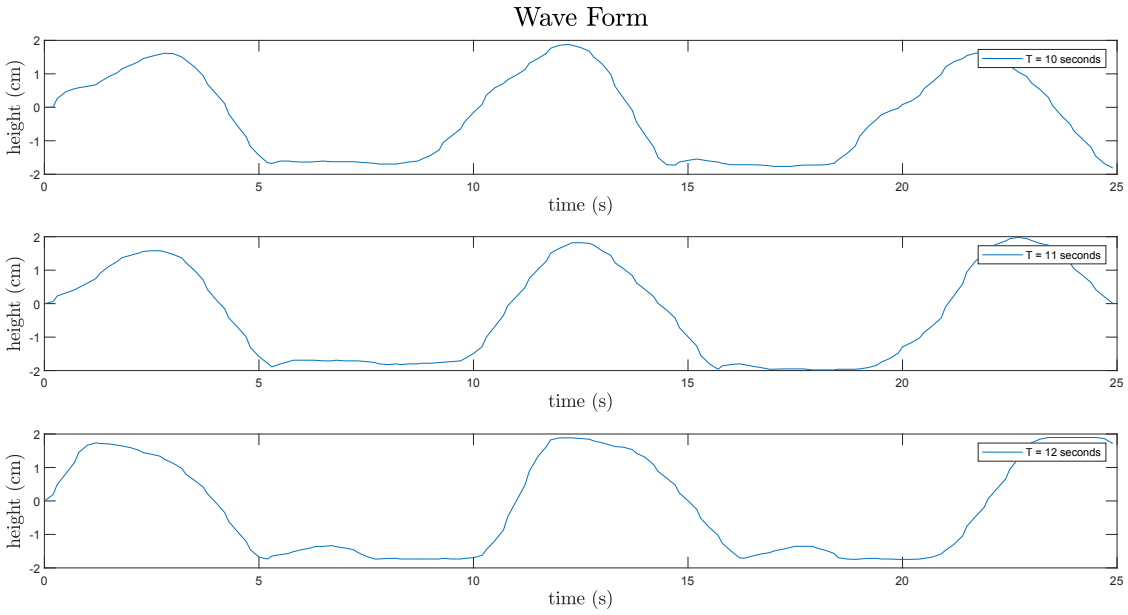

Figure 5-3.: Generations of the waves experimental.

5.2. Prototype of the WEC: Simulation Results

5.2.1. WEC Dimensioning

Once the wave behaviour is established, the dimensional parameters of the WEC are obtained by the application of Equation 4-3. Thus, the values of each of the components are presented in table **5-2**. Note that it is included the buoy radius, although the procedure of the buoy is not presented, for the mechanism in a laboratory scale the buoy was selected to ensure the sufficient load to move the dispositive.

Parameter	Value (m)
Buoy radius	0.050
Crank length	0.015
Connecting Rod length	0.070

Table 5-2.: Lengths of crank and connecting rod of WEC

5.2.2. WEC optimization

The process of optimization is conducted by minimizing Equation 4-4, and considering the following restrictions for the mass and inertia of each component:
Mass of the crank

$$1 \times 10^{-4}\,\mathrm{K}g < m_1 < 2 \times 10^{-3}\,\mathrm{K}g$$

Mass of the connecting rod

$$1 \times 10^{-4}\,\mathrm{K}g < m_2 < 1.23 \times 10^{-3}\,\mathrm{K}g$$

Inertia of the crank

$$1 \times 10^{-5}\,\mathrm{K}g.m^2 < I_1 < 5 \times 10^{-3}\,\mathrm{K}g.m^2$$

Inertia of the connecting rod

$$1 \times 10^{-7}\,\mathrm{K}g.m^2 < I_2 < 8 \times 10^{-6}\,\mathrm{K}g.m^2$$

Those limits were selected considering PLA as the WEC material, and obtaining an approximation of the minimum requirements of material given by the 3d printer. Then, using the optimization toolbox of MATLAB [63] the inertias and the masses of each component of the WEC are presented in table **5-3**. The MATLAB code is available in Appendix C.

Parameter	Value
Crank mass	$1.044\,39 \times 10^{-3}\,\mathrm{K}g$
Connecting rod mass	$2.092 \times 10^{-4}\,\mathrm{K}g$
Crank inertia	$1.045 \times 10^{-4}\,\mathrm{K}g.m^2$
Connecting rod inertia	$1.983 \times 10^{-6}\,\mathrm{K}g.m^2$
Input force average	$0.112\,\mathrm{N}$

Table 5-3.: Optimized mass and inertia of the WEC links

5.2.3. Design of the components of the WEC

According to the results obtained in Table **5-3**, the final designs of the connecting rod and connecting rod make using Solidworks are shown in Figure **5-4**. Note that,

as previously mentioned, the selected material is PLA, due to the versatility and strength suitable for a model in laboratory scale [64].

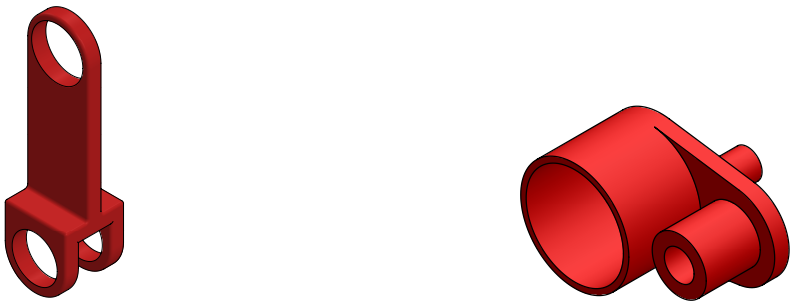

(a) Final design of connecting rod. (b) Final design of crank.

Figure 5-4.: Final design of the links of the WEC.

Finally, in Figure **5-5** shows the final design of the wave energy prototype. The design of the prototype was according to the final design of each link of the WEC and the characteristics of the wave generated in the wave tank.

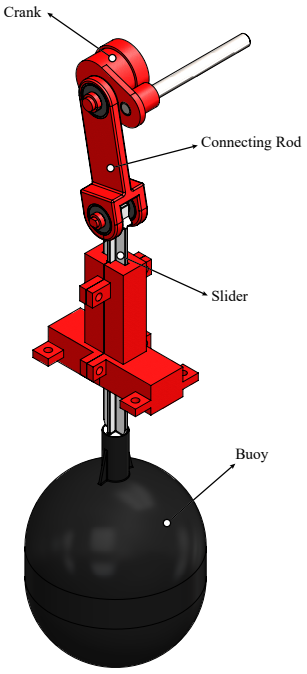

Figure 5-5.: Final design of WEC.

5.3. Electric output power of the DC generator

The selected DC generator model is DME33SA. The technical specifications are represented in Table 1. Dc Generator Specification is available in Appendix D.

Parameter	Value
Voltage	12V
Current	0.05A
Armature resistance	40Ω
Generator speed (No load)	$5500\frac{rad}{min}$

Table 5-4.: Dc Generator Specification.

According to the parameters of the Table **5-4**, the K_e variable is calculated using the Equation 4-13,

$$K_e = \frac{e_a - R_a i_a}{\omega} = 0.11V\frac{rad}{seg} \tag{5-1}$$

Now, the average torque generated by the WEC in each one of the wave period is registered in the next table,

Period (s)	τ_{wec}
10	$1.27 \times 10^{-8}\,\mathrm{N} \cdot m$
11	$1.05 \times 10^{-8}\,\mathrm{N} \cdot m$
12	$0.90 \times 10^{-8}\,\mathrm{N} \cdot m$

Table 5-5.: Average torque generated by the WEC.

Likewise, the voltages and currents generated are calculated, and they are registered in the next tables,

Period (s)	i_{wec} (mA)	e_{wec} (V)
10	7.80	0.070
11	6.44	0.063
12	5.42	0.058

Table 5-6.: Levels of electric current and voltage in the DC generator.

Finally, in Table **5-7** the results of average electrical power with different load capacity is presented.

Period (s)	$P_{Load}(mW)$ **Load: 5.7 Ω**	$P_{Load}(mW)$ **Load: 7.8 Ω**	P_{Load} (mW) **Load: 12.5 Ω**
10	0.85	0.63	7.79
11	0.70	0.51	7.25
12	0.60	0.98	7.10

Table 5-7.: Results of average electrical power with the loads of 5.7Ω, 7.8Ω and 12.5 Ω.

5.4. Experimentation

Thus, the mechanism is built and installed in the wave tank to analyze its behaviour as presented in Figure **5-6** and Figure **5-7**.

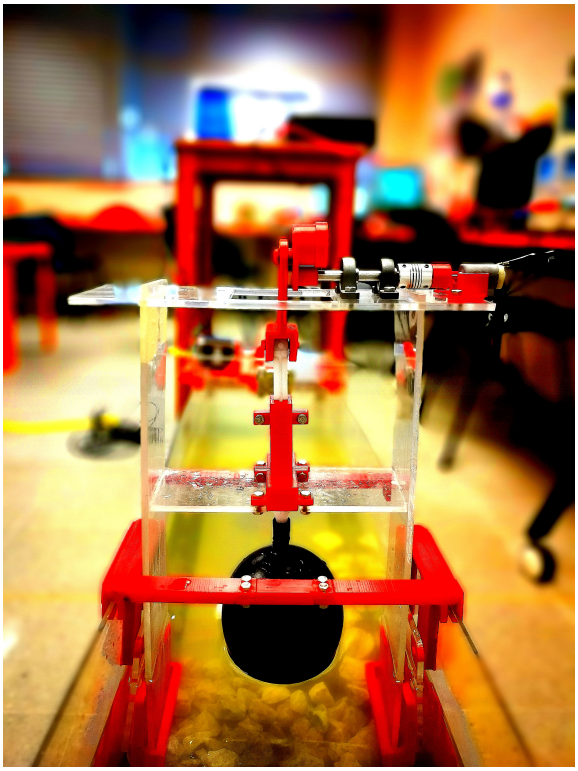

Figure 5-6.: Prototype of the WEC.

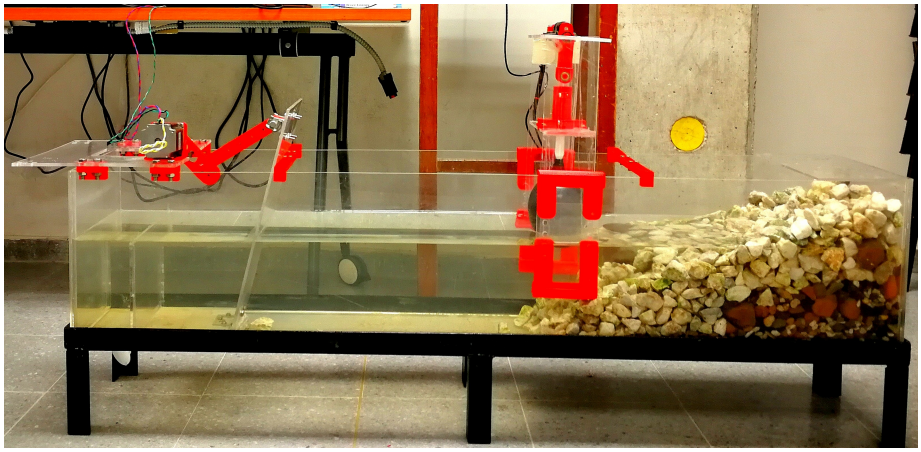

Figure 5-7.: Wave Tank.

The position of the WEC within the tank is presented in Figure **5-8** . Thus, the experimental condition are presented in the following:

- The WEC position does not vary.
- The density of the water remained constant.
- Depth of filling of the experimentation tank remained constant.
- The stepper motor speed maintains a constant rotation throughout the experimentation.
- The voltage is measured with a reference oscilloscope Tektronix TBS1062. For measuring the voltage, a differential measurement was made.
- The loads used for current measurement were 5.7 Ω, 7.8 Ω and 12 Ω. These were varying from the generated wave period.
- The Amount of data obtained throughout the experiment was the same in all cases.

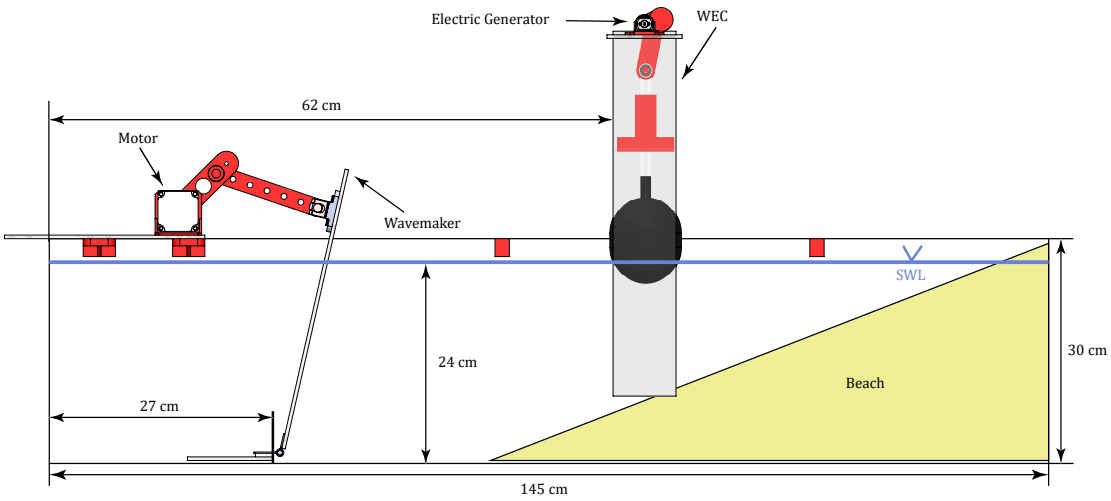

Figure 5-8.: Wave tank and Prototype.

5.4.1. Results

The results obtained in the process of the experimentation are analyzed and presented below.

Open circuit Voltage

Figure **5-9** shows the behaviour of the voltage to electric generator output in different periods of the wave and in Table **5-8**, the average tension obtained per period.

Period (s)	Voltage (V)
10	0,113
11	0,111
12	0,108

Table 5-8.: Average of the Voltage in different periods.

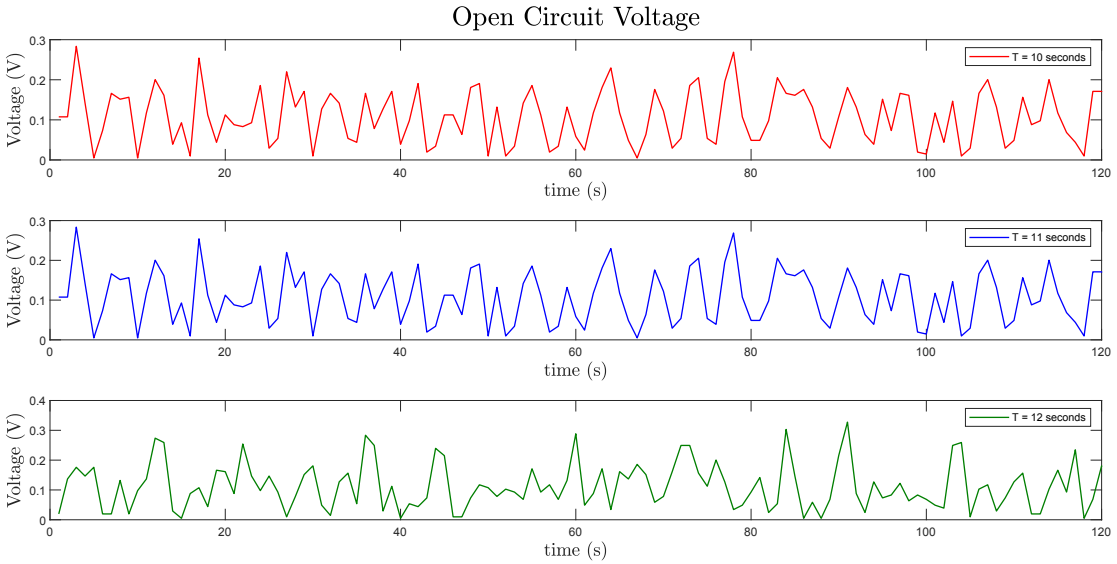

Figure 5-9.: Generations of the voltage in the DC generator.

The irregularity in the voltage by each cycle is due to the rotational movement of the slider-crank mechanism. The WEC does not produce a constant angular velocity to the output since the buoy and waves are not be in resonance. However, the dispositive is capable of maintain is rotations counter clock wise.

Loads of 5.7 Ω, 7.8 Ω and 12.5 Ω with periods of 10, 11 and 12 seconds

Figure **5-10**, **5-11** and **5-12** shows the behaviour of the electrical power varying the load capacity. Additionally, Table **5-9** presents the average electrical power.

Period (s)	**Electric power**(mW) **Load: 5.7 Ω**	**Electric power** (mW) **Load: 7.8 Ω**	**Electric power** (mW) **Load: 12.5 Ω**
10	0.70	0.62	7.10
11	1.01	0.68	7.06
12	0.74	1.20	7.28

Table 5-9.: Levels of average electrical power with the loads of 5.7Ω, 7.8Ω and 12.5 Ω.

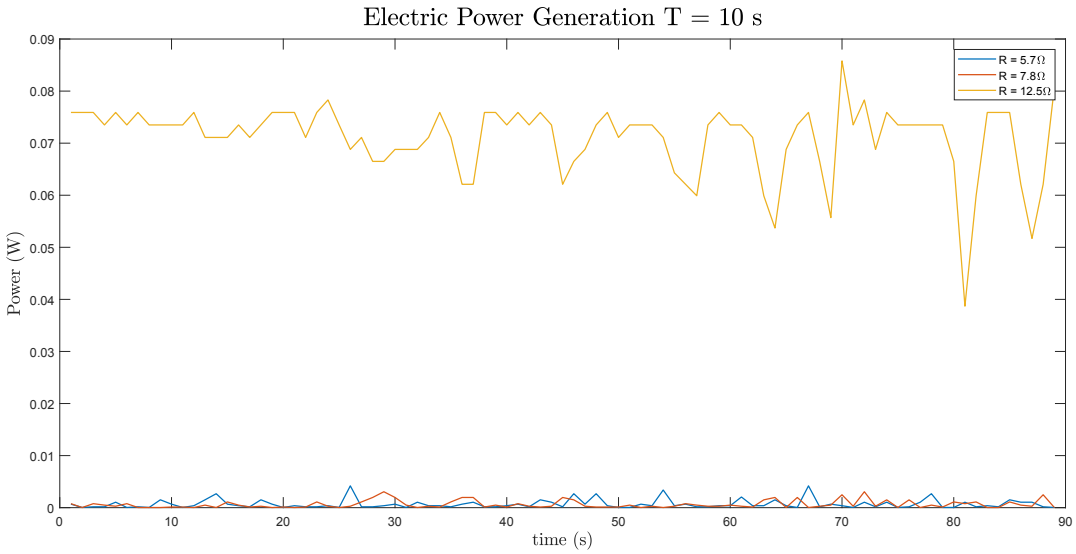

Figure 5-10.: Electric power generation with different load capacity and a wave period of 10 seconds.

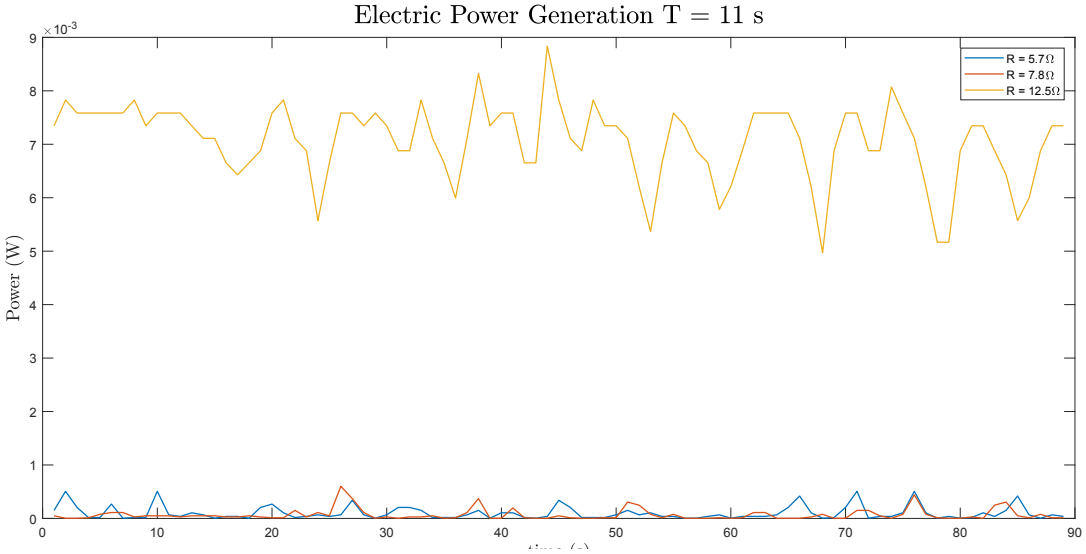

Figure 5-11.: Electric power generation with different load capacity and a wave period of 11 seconds.

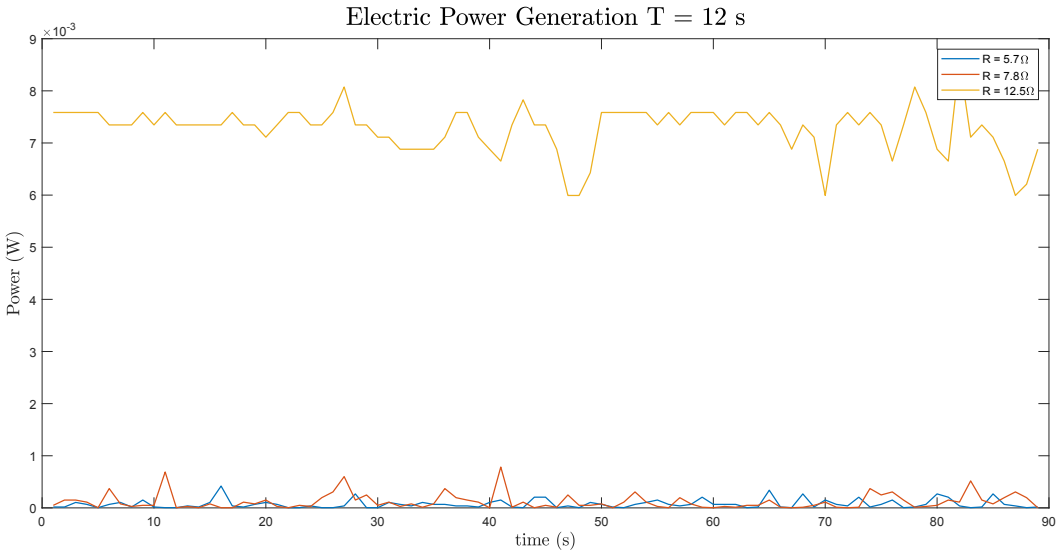

Figure 5-12.: Electric power generation with different load capacity and a wave period of 12 seconds.

The resistance of 12 Ω has greater power in comparison to the ones of 5.7 Ω and 7.8 Ω due to the greater current circulation that circulates by the load and the variation of the wave period. However, in all cases of experimentation, it was possible to generate electric power. It is possible to optimize the results by selecting higher resistance in the dispositive.

Finally, in Tables **5-10**, **5-11** and **5-12** are records the errors obtained between the simulated values and experimentation data,

Period (s)	**Electric power**(mW) **Load: 5.7 Ω Simulated**	**Electric power** (mW) **Load: 5.7 Ω Experimentation**	**Error** (%)
10	0.70	0.85	17.6
11	1.01	0.70	30.7
12	0.74	0.60	18.9

Table 5-10.: Comparison between simulated values and testing values $R_{Load} = 5.7\Omega$.

Period (s)	**Electric power**(mW) **Load: 7.8** Ω **Simulated**	**Electric power** (mW) **Load: 7.8** Ω **Experimentation**	**Error** (%)
10	0.62	0.63	1.6
11	0.68	0.51	25.0
12	1.20	0.98	18.3

Table 5-11.: Comparison between simulated values and testing values $R_{Load} = 7.8\Omega$.

Period (s)	**Electric power**(mW) **Load: 12.5**Ω **Simulated**	**Electric power** (mW) **Load: 12.5** Ω **Experimentation**	Error (%)
10	7.10	7.79	8.85
11	7.06	7.25	2.62
12	7.28	7.10	2.47

Table 5-12.: Comparison between simulated values and testing values $R_{Load} = 12.5\Omega$.

6. Conclusions

This thesis is based on renewable energy resources, more specifically wave energy, which year after year is creating more interest among researchers as a resource with excellent energy potential. For this reason, countries such as the United Kingdom and Norway have generated a constant development in this type of technology, managing to promote research on construction and technological advancement. However, research continues on the strengthening of the different mechanisms currently used in WECs and in the search for better-performing and low-cost design alternatives to generate competitiveness with other types of renewable technology. Therefore, this master's thesis proposed a methodology for designing a point converter of the type of sliding crank.

From the results obtained, it is possible to conclude the following:

- It was possible to obtain a methodology that allows the generation of energy from a WEC. The approach is based on the utilization of dynamical equations to dimension a slider-crank mechanism, through the minimization of the input force. The methodology was tested on a prototype of the device that showed the dynamic capabilities of the system.
- Improvements in the methodology should consider the implementation of a theory for the design of materials that allows the utilization of more restrictions into the optimization.
- In addition to the methodology, the dimensioning of the buoy and the selection of optimal generator should be taken into consideration for futures improvements.
- The prototype should be tested with irregular waves, to analyze its behaviour in a general scenario that emulates the conditions of the ocean.

6.1. Afterwards

Below is shown the future work of this experimentation to improve the WEC efficiency to and transform the rotational movement of the crank to a continuous one.

1. Improve the crank system and optimize the counterweight to make a continuous rotational movement.
2. Make a system of multiple buoys to improve the absorbent energy of the generator.
3. Study the different shapes the buoy can get to improve the excitation force.
4. Program the wave tank for irregular waves.
5. Add a gearbox system in the WEC to increase the Rpm at the begin of the generator to produce more energy.

Appendix

A. Irregular Waves

According to the Wave's linear theory, the ocean description can be a combination or overlap of a large number of regular sinusoidal wave components with different frequencies, heights and directions, whose surface reconstruction can be as a sum of variable amplitudes, called spectral analysis. In Figure **A-1** shows the relation between a long-crested wave power spectrum, where such a relationship can be observed. The spectrum does not provide the exact description of the ocean, but the statistical parameters that describe its characteristics. If these parameters are measured, you can define your spectrum.

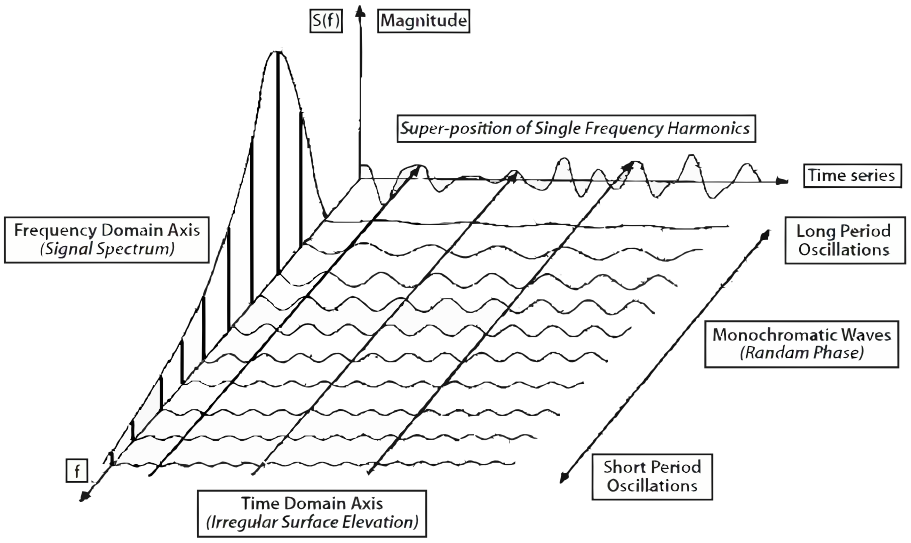

Figure A-1.: Waves in the frequency and time domain [65].

Mathematically, the spectral analysis is based on the Fourier Transform (FT) of the variation of the oceanic surface, which consists in converting the waves records concerning time in the wave spectrum, where energy is related to frequency. Thus, the division of the irregular waves are analyzed by the harmonic components.

The wave spectrum is the Spectral Density of Power (SDP) of the elevation of the surface of the sea. In the specific literature it can be found in two forms: $E(f)$, in function of the frequency (Hz) or $S(\omega)$, in function of angular frequency (rad/s) [66]. SDP describes the distribution of the sea surface energy in the frequency domain. A narrow-band spectrum represents a regular sea of state, where most of the power concentration in the waves of the same frequency. On the other hand, a large-area wave spectrum represents an ocean with large waves, laughing at a chaotic sea of state, with mixtures of short and long waves.

A.0.1. Wave records

A typical wave record measured by a wave-meter buoy that represent the real sea state can be observed in the next Figure **A-2**.

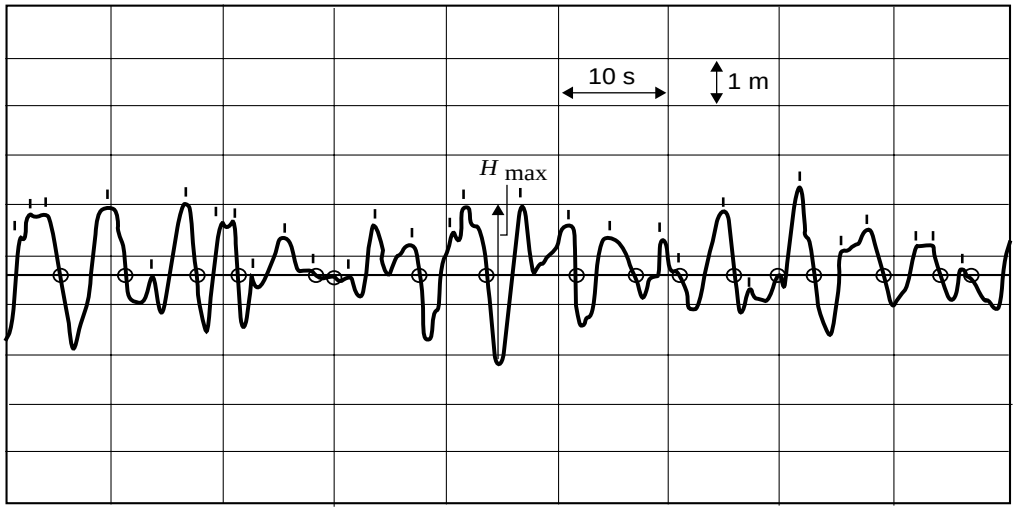

Figure A-2.: Sample of a wave record [54].

Compared with Figure **3-2**, the waveform is entirely different, which leads to make two assumptions: First, the measured waveform record is never repeated precisely because of the random appearance of the sea surface; second, the state of the sea is "stationary ", the statistical properties of the distribution of heights and periods will have similarities between them. From the above, the most appropriate parameters for describing the sea status of a measured wave record are therefore statistical.

A.0.2. Wave spectrum

The region of the ocean in which wind blows is known, in literature, as fetch. A wind that blows steadily for a certain period in an ocean of unlimited fetch can be considered statically stable. Such characteristics define a fully developed sea.

If the waves propagate in the dominant direction of the wind, then the ridges are predominantly unidirectional. In other words, the shape of each wave does not change between vertical planes parallel to each other and with the dominant direction. These waves type are known as irregular long-crested waves. For another hand, when irregularities are presented not in one, but in several courses of wind, the type sea is recognized by the name of irregular short-crested wave.

Many spectrums maintain the shape of Equation A-1. They differ as to the parameters used to determine A and B, as can be seen in Table **A-1**. Among other spectrums included in the Bretschneider Spectrum family is the TMA, for finite-depth waters, the JONSWAP, for limited fetch, and the Ochi & Hubble, for wave energy concentrations in two different frequency ranges [67].

Stansberg et al. [67] mention that for floating stationary systems, it is of paramount importance the parameters of significant height and peak period, therefore the study carried out was done under these parameters.

$$E(f) = \frac{A}{f^{-5}} \cdot \exp -B/f^4 \tag{A-1}$$

Spectrum	**A and B defined by:**
Pierson-Moskowitz (one parameters)	Significant wave height or wind speed or peak period.
Pierson-Moskowitz (two parameters)	Significant wave height and peak period.
ITTC	Signicante Wave height and Energy period or peak period or average period or zero-step period.

Table A-1.: Parameters used to evaluate the constants of the Bretschneider spectrum.

A.0.3. Model forms for wave spectrum

The different spectrum used to model the state of the sea are explained below.

1. **Pierson-Moskowitz spectrum**

   The Pierson-Moskowitz spectrum is used to model a fully developed sea. This Spectrum comes from the measurement and selection of 420 types of waves with the Shipborne Wave Recorder — developed by Tucker (1956) on board British Ocean weather ships during the five-year period 1955 – 1960. The Equation A-2 represents this model,

   $$E(f) = \frac{\alpha g^2}{(2\pi)^4 f^5} e^{-0.74\left(\frac{g}{2\pi u f}\right)} \tag{A-2}$$

   where $E(f)$ is the variance density (in m^2/s), f the wave frequency (Hz), u the wind speed (m/s) at 19.5 m above the sea surface, g the gravity (in m/s^2) and α a dimensionless quantity, $\alpha = 0.0081$.

   The Equation A-3 represents the peak of the frequency of the Pierson-Moskowitz spectrum,

   $$f_p = 0.877 \frac{g}{2\pi u} \tag{A-3}$$

   and for the calculation of the significant wave height, is represented in the Equation A-4 with the variable H_{m0} for a fully grown sea is,

   $$H_{m0} = 0.0246 u^2 \tag{A-4}$$

2. **Phillips' spectrum**

   This model describes the high-frequency part of the spectrum, above the spectral peak. It recognizes that the logarithm of the spectrum is generally close to a straight line, with a slope that is about –5. The Equation A-5 represents this model,

   $$\begin{aligned} E(f) &= 0.005 \tfrac{g^2}{f^5}, \quad if\ f \geq \tfrac{g}{u} \\ E(f) &= 0 \qquad\qquad elsewhere. \end{aligned} \tag{A-5}$$

3. **JONSWAP spectrum**

It is often used to describe waves in a growing phase. The equation that represents the spectrum use the terms of the peak frequency instead than the wind speed, described in Equation A-6,

$$E(f) = \frac{\alpha g^2}{(2\pi)^4 f^5} e^{-1.25\left(\frac{f}{f_p}\right)^4} \gamma(f) \tag{A-6}$$

The function γ is the peak enhancement factor. This factor modifies the interval around the spectral peak, generating a sharper form that in the Pierson-Moskowitz spectrum, see Figure **A-3**.

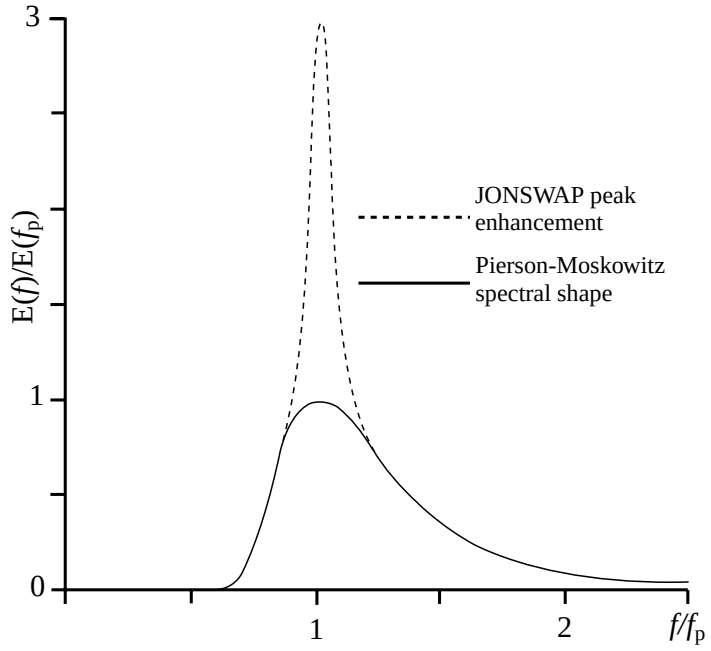

Figure A-3.: JONSWAP spectrum as a function of f/f_p [54].

From JONSWAP results, a relation is proposed between wave variance and peak frequency for a wide range of growth stages. The Equation A-7 obtained, in terms of H_m0 and F_p, is represented as,

$$H_{m0} = 0.0414 f_p^{-2} (f_p u)^{1/3} \tag{A-7}$$

The peak frequency can be obtained by reversing Equation A-8,

$$f_p = 0.148 H_{m0}^{-0.6} u^{0.2} \tag{A-8}$$

The previous equation is handy when estimating the approximate spectrum and the characteristic of the wave period when the wave height and wind velocity are known.

4. **TMA (Texel-Marsen-Arsloe) spectrum**

   This spectrum has the main characteristic of being modeled at limited water depths, described in Equation A-9,

$$E(f) = E_{JONSWAP}(f)\phi(f, h) \tag{A-9}$$

   where ϕ is a function of frequency, f, and depth, h.

B. Design Plans

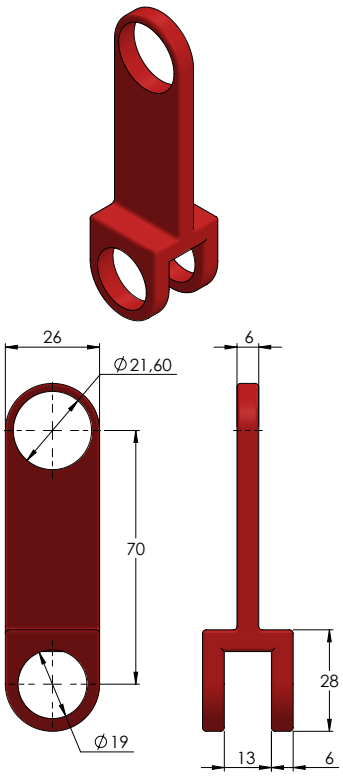

Figure B-1.: Connecting Rod.

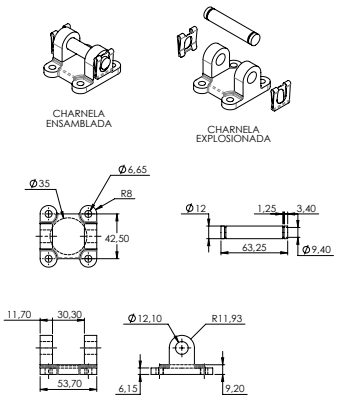

Figure B-2.: Charnela.

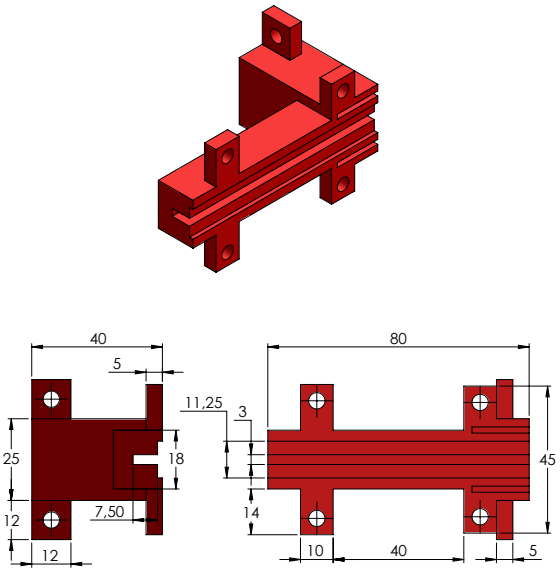

Figure B-3.: Support of Connecting Rod

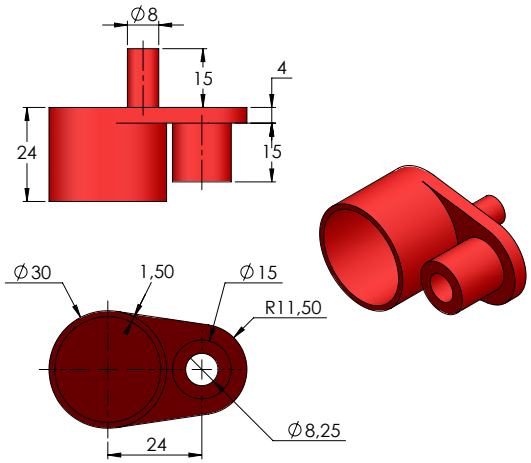

Figure B-4.: Crank.

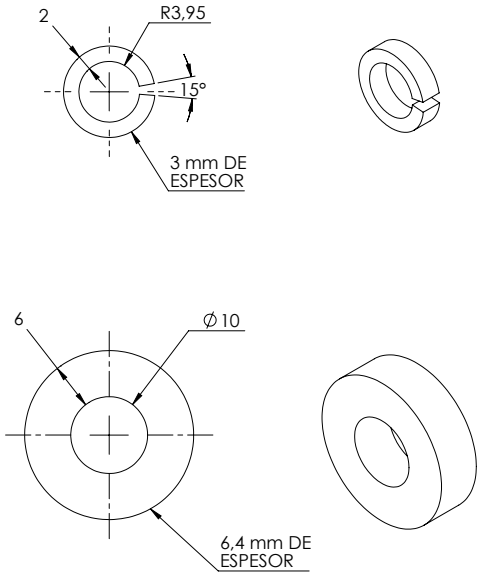

Figure B-5.: stop.

C. Code

```
% Primera prueba de simulaci n convertidor de olas
% 4-04-2019

clear all
clc
close all
%% Variable

% a:      ngulo  entre la biela y centro de masa (  )
% t1,th1:     ngulo  de la manivela.       (  )
% td1:  Velocidad de la manivela.        (m/s)
% tdd1: Aceleraci n de la manivela.      (m/s^2)
% t2,th2:     ngulo  de la corredera.      (  )
% td2:  Velocidad de la corredera.       (m/s)
% tdd2: Aceleraci n de la corredera.     (m/s^2)
% L1:   Longitud de la manivela.         (m)
% L2:   Longitud de la corredera.        (m)
% q:    Posici n de la boya.             (m)
% qd:   Velocidad de la boya.            (m/s)
% qdd:  Aceleraci n de la boya.          (m/s^2)
% L3:   Vector resultante (Posici n de la boya respecto
   al origen)  (m)
% t:    Tiempo.                          (s)
% g:    Gravedad.                        (m/s^2)
% mb:   Masa de la manivela.             (Kg)
% M2:   Masa de la biela.                (Kg)
% I1:   Inercia de la manivela.          (Kg.m^2)
% I2:   Inercia de la biela.             (Kg.m^2)
% M:    Momento inercial del sistema biela manivela.(Kg.m
   ^2)
% Tm:   Torque del generador el ctrico. (Newton.m)
```

```
30 % Wm:   Velocidad angular del generador el ctrico. (rad/s
       )
31 % I:     Corriente el ctrica del generador.          (A)
32 % V:     Voltaje del generador el ctrico.            (V)
33 % h_max: Amplitud m xima de la ola.                  (m)
34 % F:     Fuerza de extracci n de ola.                (N)
35
36 syms L3 L2 L1 LI t t2 t1 F M I1 I2 m2 mb g a q qd qdd
37
38 F_obj=solve(-(L1^2*L2^3*M*sin(t1 - t2)^3*sin(t2) - I2*L1
       ^3*sin(t1)^3*qd^2*cos(t1 - t2) - I1*L2^3*sin(t2)^3*qd
       ^2*cos(t1 - t2) - F*L1^3*L2^3*sin(t1 - t2)^4 + L1^3*L2
       ^3*g*m2*sin(t1 - t2)^4 + L1^3*L2^3*g*mb*sin(t1 - t2)^4
       + L1^3*L2^3*m2*qdd*sin(t1 - t2)^4 + I1*L1*L2^3*qdd*sin(
       t1 - t2)^2*sin(t2)^2 + I2*L1^3*L2*qdd*sin(t1 - t2)^2*
       sin(t1)^2 - L1^3*LI^2*m2*sin(t1)^3*cos(a - t2)^2*qd^2*
       cos(t1 - t2) - I1*L1*L2^2*sin(t1)*sin(t2)^2*qd^2*cos(t1
        - t2) - I2*L1^2*L2*sin(t1)^2*sin(t2)*qd^2*cos(t1 - t2)
        - L1^3*LI^2*m2*sin(t1)^3*sin(a - t2)^2*qd^2*cos(t1 -
       t2) - 2*L1^3*L2^2*LI*m2*qdd*sin(t1 - t2)^3*sin(t1)*cos(
       a - t2) + L1^3*L2*LI^2*m2*qdd*sin(t1 - t2)^2*sin(t1)^2*
       cos(a - t2)^2 + L1^3*L2*LI^2*m2*qdd*sin(t1 - t2)^2*sin(
       t1)^2*sin(a - t2)^2 - I1*L1*L2^2*sin(t1 - t2)*cos(t2)*
       sin(t1)*sin(t2)*qd^2 + I2*L1^2*L2*sin(t1 - t2)*cos(t1)*
       sin(t1)*sin(t2)*qd^2 + L1^3*L2*LI*m2*sin(t1 - t2)^2*sin
       (t1)^2*sin(a - t2)*qd^2 - L1^3*L2^2*LI*g*m2*sin(t1 - t2
       )^3*sin(t1)*cos(a - t2) - L1^2*L2^2*LI*m2*sin(t1 - t2)
       ^2*cos(t1)*sin(t2)*cos(a - t2)*qd^2 + L1^3*L2*LI*m2*sin
       (t1 - t2)*sin(t1)^2*cos(a - t2)*qd^2*cos(t1 - t2) - L1
       ^2*L2*LI^2*m2*sin(t1)^2*sin(t2)*cos(a - t2)^2*qd^2*cos(
       t1 - t2) - L1^2*L2*LI^2*m2*sin(t1)^2*sin(t2)*sin(a - t2
       )^2*qd^2*cos(t1 - t2) + L1^2*L2*LI^2*m2*sin(t1 - t2)*
       cos(t1)*sin(t1)*sin(t2)*cos(a - t2)^2*qd^2 + L1^2*L2*LI
       ^2*m2*sin(t1 - t2)*cos(t1)*sin(t1)*sin(t2)*sin(a - t2)
       ^2*qd^2 + L1^2*L2^2*LI*m2*sin(t1 - t2)*sin(t1)*sin(t2)*
       cos(a - t2)*qd^2*cos(t1 - t2))/(L1^3*L2^3*sin(t1 - t2)
       ^4),F);
39 C=coeffs(F_obj,[qdd,qd],'All');
```

```
40
41 % Coeficientes de la ecuaci n diferencial
42 A1=C(1,3);
43 A2=C(2,1);
44 A3=C(2,3);
45
46 %% Valores de las variables
47 n = 3;  % N mero de vueltas
48 l1= 0.015;
49 l2= 0.07;
50 li=l1;
51 % T= 9.99;           % Perido de la ola
52 % T= 11;           % Perido de la ola
53  T= 11.99;           % Perido de la ola
54 w= 2*pi/T;
55 h_max=l1;
56 gr= 9.8;
57 % Mb= 0.006;        % referencia con referencia PET
58 % M2= 0.00523;      % referencia con referencia PET
59 % i1= 5.4000e-02; % referencia con referencia PET
60 % i2= 8.2e-6;       % referencia con referencia PET
61 Mb = 0.001855782415826;      % Valor optimizado
62 M2 = 0.001228315905464;      % Valor optimizado
63 i1 = 0.000010002875817;      % Valor optimizado
64 i2 = 0.000001882910210;      % Valor optimizado
65
66
67
68 % Velocidad angular de la manivela
69 ve_man = (sin(t2)*qd)/(L1*sin(t1 - t2));
70
71 % Aceleraci n angular de la manivela
72 ac = -(L2*sin(t2)^2*qd^2*cos(t1 - t2) - L1*L2*qdd*sin(t1 -
       t2)^2*sin(t2) + L1*sin(t1 - t2)*cos(t2)*sin(t1)*qd^2 +
       L1*sin(t1)*sin(t2)*qd^2*cos(t1 - t2))/(L1^2*L2*sin(t1
      - t2)^3); % Aceleraci n angular de la manivela
73
74 %% C lculo de los  ngulos
```

```
75
76  [l3,t2_1,t1_1,y,yd,ydd,B] = Angle(l1,l2,T,n);
77
78  th1 = t1_1;          %  ngulo  de la manivela
79  th2 = t2_1;          %  ngulo  de la biela
80  alpha= th1;
81
82  % Velocidad y aceleraci n de la boya vs ola
83  q_bouy = y;          % Posici n de la ola
84  qd_1  = yd;          % Velocidad de la ola
85  qdd_1 = ydd;         % Aceleraci n de la ola
86
87  N = length(th1);
88  for i = 1:N
89
90  %% car cteristicas del motor
91
92  % Referencia del motorreductor dc Nema 17
93  % https://www.vistronica.com/robotica/motores/motor-paso-a
       -paso/motor-paso-a-paso-5-6kgcm-nema-17-para-impresora
       -3d-detail.html
94  %
95  % Ke: Constante de fuerza electromotriz (FCEM) del motor [
       V/rad.s-1]
96  % Vb: Fuerza contraelectromotriz (FCEM) debido al giro del
        motor [V]
97
98  % t_m = 0.5491724;   % Torque Nominal de motor dc [Nm]
99  % w_m(i) = eval(subs(ve_man,{L1,t1,t2,qd},{l1,th1(i),th2(i
       ),qd_1(i)})); % Se pasa de RPM a rad/s (vel de la
       manivela)
100 % v = 3;             % Tensi n de operaci n 6 a 12 VDC
101 % I = 0.04;          % Corriente a 12v sin carga [A]
102 %
103 % % Link de las formulas: https://repository.upb.edu.co/
       bitstream/handle/20.500.11912/504/digital_17633.pdf?
       sequence=1
104 % Ke = v/w_m(i);
```

```
105 %
106 % Ra = 2;          % Resistencia de armadura [ohm]
107 % La = 2.8e-3 ;    % Inductancia de armadura [H]
108 % te = La/Ra;      % Constante de tiempo el ctrica [s]
109 %
110 % Kt = t_m/I;       % Relaci n directa del par conla
    corriente inducida [Nm/A]
111 % tm = 15e-3;       % Constante de tiempo mec nica [s]
112 %
113 % Jm = (tm*Kt)*Ke/Ra; % Momento inercial del motor [Kg.m2]
114 %
115 % Mr = 1;            % Masa de la carga [kg]
116 % efi = 0.98;        % Eficiencia del motor
117 %
118 % iop = (Mr/(efi*Jm))^1/2; % Relaci n de transmisi n
    ptima   [m-1]
119 %
120 % Je(i) = Jm + Mr/(efi*iop)^2; % Momento de intercia
    equivalente en ell eje del motor [Kg-m2]
121
122 Je = 7e-8; % Inercial del eje del motor de paso longitud
    70 mm largo y 6 mm de diametro.
123 %% Evaluar los valores
124
125 % Aceleraci n de la manivela
126   ac = eval(subs(ac,{L1,L2,t1,t2,qd,qdd},{l1,l2,th1(i),th2
        (i),qd_1(i),qdd_1(i)}));
127   ve(i) = eval(subs(ve_man,{L1,t1,t2,qd},{l1,th1(i),th2(i)
        ,qd_1(i)}));
128   ac_man(i) = Je.*ac + 2e-4*ve(i);
129
130 % Coeficiente de la ecuaci n diferencial
131   A1=eval(subs(A1,{L1,L2,LI,m2,mb,t1,t2,a,g,I1,I2},{l1,l2,
        li,M2,Mb,th1(i),th2(i),alpha(i),gr,i1,i2}));
132   A2=eval(subs(A2,{L1,L2,LI,m2,t1,t2,a,I1,I2},{l1,l2,li,M2
        ,th1(i),th2(i),alpha(i),i1,i2}));
133   A3=eval(subs(A3,{L1,L2,LI,M,m2,mb,t1,t2,a,g},{l1,l2,li,
        ac_man(i),M2,Mb,th1(i),th2(i),alpha(i),gr}));
```

```
134
135 % Fuerza
136   Force (i) = A1*qdd_1(i) + A2*qd_1(i) + A3;
137
138 end
139
140 % Gr ficas
141
142 % hold on
143 % figure (1)
144 % subplot (2,1,1)
145 % plot (Force)
146 % title('Input Force of the System', 'Interpreter', 'latex
      ','FontSize', 20);
147 % ylabel('Force (N)', 'Interpreter', 'latex', 'FontSize',
      14);
148 % xlabel('time (Seg)', 'Interpreter', 'latex', 'FontSize',
       14);
149 %
150 % subplot (2,1,2)
151 % plot (y)
152 % title('Wave Position', 'Interpreter', 'latex','FontSize
      ', 20)
153 % ylabel('height (m)', 'Interpreter','latex','FontSize',
      14);
154 % xlabel('time (Seg)', 'Interpreter', 'latex','FontSize',
      14);
155 %
156 %
157 % % Wave characteristic
158 % figure (2)
159 % subplot (3,1,1)
160 % plot (y)
161 % title('Wave position', 'Interpreter', 'latex','FontSize
      ', 20);
162 % ylabel(' height (m)', 'Interpreter', 'latex', 'FontSize
      ', 14);
```

```
163 % xlabel('time (Seg)', 'Interpreter', 'latex', 'FontSize',
      14);
164 %
165 % subplot (3,1,2)
166 % plot (yd)
167 % title('Wave velocity', 'Interpreter', 'latex','FontSize
    ', 20);
168 % ylabel('Velocity (m/s)', 'Interpreter', 'latex', '
    FontSize', 14);
169 % xlabel('time (Seg)', 'Interpreter', 'latex', 'FontSize',
      14);
170 %
171 % subplot (3,1,3)
172 % plot (ydd)
173 % title('Wave acceleration', 'Interpreter', 'latex','
    FontSize', 20);
174 % ylabel('Acceleration (m/s2)', 'Interpreter', 'latex', '
    FontSize', 14);
175 % xlabel('time (Seg)', 'Interpreter', 'latex', 'FontSize',
      14);
176 %
177 % % Crank characteristic
178 % figure (3)
179 % subplot (3,1,1)
180 % plot (y)
181 % title('Crank position', 'Interpreter', 'latex','FontSize
    ', 20);
182 % ylabel(' height (m)', 'Interpreter', 'latex', 'FontSize
    ', 14);
183 % xlabel('time (Seg)', 'Interpreter', 'latex', 'FontSize',
      14);
184 %
185 % subplot (3,1,2)
186 % plot (ve)
187 % title('Crank velocity', 'Interpreter', 'latex','FontSize
    ', 20);
188 % ylabel('Velocity (m/s)', 'Interpreter', 'latex', '
    FontSize', 14);
```

```
189 % xlabel('time (Seg)', 'Interpreter', 'latex', 'FontSize',
        14);
190 %
191 % subplot (3,1,3)
192 % plot (ac_man)
193 % title('Crank acceleration', 'Interpreter', 'latex','
       FontSize', 20);
194 % ylabel('Acceleration (m/s2)', 'Interpreter', 'latex', '
       FontSize', 14);
195 % xlabel('time (Seg)', 'Interpreter', 'latex', 'FontSize',
        14);
196
197 %
       ================================================================

198 %
       ================================================================

199 %% Optimizaci n
200 F_op=solve(-(L1^2*L2^3*M*sin(t1 - t2)^3*sin(t2) - I2*L1^3*
       sin(t1)^3*qd^2*cos(t1 - t2) - I1*L2^3*sin(t2)^3*qd^2*
       cos(t1 - t2) - F*L1^3*L2^3*sin(t1 - t2)^4 + L1^3*L2^3*g
       *m2*sin(t1 - t2)^4 + L1^3*L2^3*g*mb*sin(t1 - t2)^4 + L1
       ^3*L2^3*m2*qdd*sin(t1 - t2)^4 + I1*L1*L2^3*qdd*sin(t1 -
        t2)^2*sin(t2)^2 + I2*L1^3*L2*qdd*sin(t1 - t2)^2*sin(t1
       )^2 - L1^3*LI^2*m2*sin(t1)^3*cos(a - t2)^2*qd^2*cos(t1
       - t2) - I1*L1*L2^2*sin(t1)*sin(t2)^2*qd^2*cos(t1 - t2)
       - I2*L1^2*L2*sin(t1)^2*sin(t2)*qd^2*cos(t1 - t2) - L1
       ^3*LI^2*m2*sin(t1)^3*sin(a - t2)^2*qd^2*cos(t1 - t2) -
       2*L1^3*L2^2*LI*m2*qdd*sin(t1 - t2)^3*sin(t1)*cos(a - t2
       ) + L1^3*L2*LI^2*m2*qdd*sin(t1 - t2)^2*sin(t1)^2*cos(a
       - t2)^2 + L1^3*L2*LI^2*m2*qdd*sin(t1 - t2)^2*sin(t1)^2*
       sin(a - t2)^2 - I1*L1*L2^2*sin(t1 - t2)*cos(t2)*sin(t1)
       *sin(t2)*qd^2 + I2*L1^2*L2*sin(t1 - t2)*cos(t1)*sin(t1)
       *sin(t2)*qd^2 + L1^3*L2*LI*m2*sin(t1 - t2)^2*sin(t1)^2*
       sin(a - t2)*qd^2 - L1^3*L2^2*LI*g*m2*sin(t1 - t2)^3*sin
       (t1)*cos(a - t2) - L1^2*L2^2*LI*m2*sin(t1 - t2)^2*cos(
       t1)*sin(t2)*cos(a - t2)*qd^2 + L1^3*L2*LI*m2*sin(t1 -
```

```
   t2)*sin(t1)^2*cos(a - t2)*qd^2*cos(t1 - t2) - L1^2*L2*
   LI^2*m2*sin(t1)^2*sin(t2)*cos(a - t2)^2*qd^2*cos(t1 -
   t2) - L1^2*L2*LI^2*m2*sin(t1)^2*sin(t2)*sin(a - t2)^2*
   qd^2*cos(t1 - t2) + L1^2*L2*LI^2*m2*sin(t1 - t2)*cos(t1
   )*sin(t1)*sin(t2)*cos(a - t2)^2*qd^2 + L1^2*L2*LI^2*m2*
   sin(t1 - t2)*cos(t1)*sin(t1)*sin(t2)*sin(a - t2)^2*qd^2
    + L1^2*L2^2*LI*m2*sin(t1 - t2)*sin(t1)*sin(t2)*cos(a -
    t2)*qd^2*cos(t1 - t2))/(L1^3*L2^3*sin(t1 - t2)^4),F);
201
202 % Reemplazo de constantes en la funci n objetivo
203 F_op = subs(F_op,{L1,L2,M,g,LI},{l1,l2,Je,gr,li});
204
205 % sustituci n
206
207 % Esta sustituci n se realiza para colocar la funci n
      objetivo de la forma
208 % fun (x) = x(1) + x(2) + ... + x(n). Cada varibale a
      optimizar
209 % se representa como X(n).
210
211 % mb: x(1)
212 % m2: x(2)
213 % I1: x(3)
214 % I2: x(4)
215 % a : x(5)
216
217 % Soluci n de la optimizaci n
218 t1  = eval(subs(th1));
219 t2  = eval(subs(th2));
220 qd  = eval(subs(yd));
221 qdd = eval(subs(ydd));
222 % a   = subs(alpha);
223
224 Fun_1 = @(x,t1,t2,qd,qdd) -1*mean
   ((1000000000000.*((16807.*x(2).*sin(t1 - t2).^4)
   ./5000000000000 + (16807.*x(1).*sin(t1 - t2).^4)
   ./5000000000000 + (18141443080592030 29.*sin(t1 - t2)
   .^3.*sin(t2))./7555786372591432341913600000000000 +
```

```
   (343.*x(2).*qdd.*sin(t1 - t2).^4)./1000000000000 -
   (2401.*x(2).*sin(t1 - t2).^3.*sin(t1).*cos(x(5) - t2))
   ./5000000000000 - (343.*x(3).*qd.^2.*cos(t1 - t2).*sin(
   t2).^3)./1000000 - (x(4).*qd.^2.*cos(t1 - t2).*sin(t1)
   .^3)./1000000 + (343.*x(3).*qdd.*sin(t1 - t2).^2.*sin(
   t2).^2)./100000000 + (7.*x(4).*qdd.*sin(t1 - t2).^2.*
   sin(t1).^2)./100000000 - (x(2).*qd.^2.*cos(t1 - t2).*
   sin(t1).^3.*cos(x(5) - t2).^2)./10000000000 - (x(2).*qd
   .^2.*sin(x(5) - t2).^2.*cos(t1 - t2).*sin(t1).^3)
   ./10000000000 + (7.*x(2).*qdd.*sin(t1 - t2).^2.*sin(t1)
   .^2.*cos(x(5) - t2).^2)./1000000000000 + (7.*x(2).*qd
   .^2.*sin(x(5) - t2).*sin(t1 - t2).^2.*sin(t1).^2)
   ./10000000000 + (7.*x(2).*qdd.*sin(x(5) - t2).^2.*sin(
   t1 - t2).^2.*sin(t1).^2)./1000000000000 - (49.*x(2).*
   qdd.*sin(t1 - t2).^3.*sin(t1).*cos(x(5) - t2))
   ./500000000000 - (49.*x(3).*qd.^2.*cos(t1 - t2).*sin(t1
   ).*sin(t2).^2)./1000000 - (7.*x(4).*qd.^2.*cos(t1 - t2)
   .*sin(t1).^2.*sin(t2))./1000000 - (7.*x(2).*qd.^2.*cos(
   t1 - t2).*sin(t1).^2.*sin(t2).*cos(x(5) - t2).^2)
   ./10000000000 - (49.*x(3).*qd.^2.*sin(t1 - t2).*cos(t2)
   .*sin(t1).*sin(t2))./1000000 + (7.*x(4).*qd.^2.*sin(t1
   - t2).*cos(t1).*sin(t1).*sin(t2))./1000000 - (7.*x(2).*
   qd.^2.*sin(x(5) - t2).^2.*cos(t1 - t2).*sin(t1).^2.*sin
   (t2))./10000000000 - (49.*x(2).*qd.^2.*sin(t1 - t2)
   .^2.*cos(t1).*sin(t2).*cos(x(5) - t2))./10000000000 +
   (7.*x(2).*qd.^2.*cos(t1 - t2).*sin(t1 - t2).*sin(t1)
   .^2.*cos(x(5) - t2))./10000000000 + (49.*x(2).*qd.^2.*
   cos(t1 - t2).*sin(t1 - t2).*sin(t1).*sin(t2).*cos(x(5)
   - t2))./10000000000 + (7.*x(2).*qd.^2.*sin(t1 - t2).*
   cos(t1).*sin(t1).*sin(t2).*cos(x(5) - t2).^2)
   ./10000000000 + (7.*x(2).*qd.^2.*sin(x(5) - t2).^2.*sin
   (t1 - t2).*cos(t1).*sin(t1).*sin(t2))./10000000000))
   ./(343.*sin(t1 - t2).^4));
Fun_2 = @(x) Fun_1(x,t1,t2,qd,qdd);

% Restricciones
%
    A = [];
```

```
230     b = [];
231     Aeq = [];
232     beq = [];
233
234 %           mb       m2        I1           I2      a
235     lb  = [0.0001   0.00010   1e-5        1e-7    0   ];
236     x0  = [0.001    0.00020    1e-4        2e-6     0.1 ];
237     ub  = [0.002    0.00123    5e-03       8e-6     2*pi];
238
239 format long
240 % Minimizaci n
241 [y_1,F1] = fmincon(Fun_2,x0,A,b,Aeq,beq,lb,ub);
242               %mb     %m1     %I1     %I2     %a
243 variable = [y_1(1),y_1(2),y_1(3),y_1(4),y_1(5)];
244 F_op_min = F1;
245
246
247 % figure (2)
248 % plot (sort(F_op_min,'ascend'))
249 % title('Maximization of the Force', 'Interpreter', 'latex
    ','FontSize', 20);
250 % ylabel('Force (N)', 'Interpreter', 'latex', 'FontSize',
    14);
251 % xlabel('Iterations', 'Interpreter', 'latex', 'FontSize',
     14);
252
253
254 %% Potencia El ctrica de salida
255 % 1. Calcular los coeficientes de torque mec nico (Kt) y
256 % torque de voltaje (Ke) del generador el ctrico DC
257
258 % Datos entregados por el fabricante
259 Vel_ang_motor_dc = 91.66; % [rad/seg] Velocidad angular
    nominal del Gen DC
260 Ea = 12; % [V] Tensi n nominal a la salida del generador
    DC
261 Ra = 41; % [ohm] Resistencia del devanado de armadura
```

```
ia = 0.05; % [A] Corriente nominal del devanado de armadura

kt = (Ea - Ra*ia)/91.66; % Coeficientes de torque mec nico

% 2. Calcular el torque mec nico del convertidor Undimotriz
% Torque de la manivela  = Fuerza de la manivela X Radio de manivela
% Fuerza de la manivela = Inercia de la manivela X aceleraci n angular de
% la manivela

% Crank_Force =  mean(ac_man)* i1;

Crank_Force =  mean(ac)* i1;

l1= 0.015; % [m] Radio de la manivela

Torque_man_ave = Crank_Force*l1;

% 3. Calcular la corriente generada a partir del torque de entrada. La
% ecuaci n se saca del art culo "A study on dynamic motion and wave power in
% multi-connected wave energy converter"

Gen_DC_Current = Torque_man_ave/(l1*kt) % [1]

% 4. Calcular la tensi n generada por el generador DC
ang_vel_man = mean(ve);
% Ea_Gen_DC = (Ra*Gen_DC_Current) + (kt*ang_vel_man); % [1]
 Ea_Gen_DC = l1*kt*ang_vel_man; % [2]

% 5. Calcular la potencia el ctrica Generada
% Carga conectada al generador el ctrico
```

```
292
293 RLoad_5_7 = 5.7; % [ohm]
294 RLoad_7_8 = 7.8; % [ohm]
295 RLoad_12_5 = 12.5; % [ohm]
296
297 % [1]
298 P_Gen_RLoad_5_7 = (Ea_Gen_DC^2)/RLoad_5_7;
299 P_Gen_RLoad_7_8 = (Ea_Gen_DC^2)/RLoad_7_8;
300 P_Gen_RLoad_12_5 = (Ea_Gen_DC^2)/RLoad_12_5;
```


UN
UNIVERSIDAD
DEL NORTE
Vigilada Mineducación
UNIVERSIDAD DEL NORTE
1966
ALEGRÍA

D. DC Generator

DME33

MODEL CODE	VOLTAGE	OUTPUT	CURRENT
SA	12V	0.7W	0.12A
SB	24V	0.7W	0.06A
BA	12V	3.0W	0.42A
BB	24V	3.0W	0.22A

●DIMENSIONS Unit mm(inch)

DME33SA, DME33SB

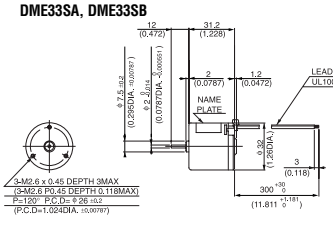

DME33BA, DME33BB

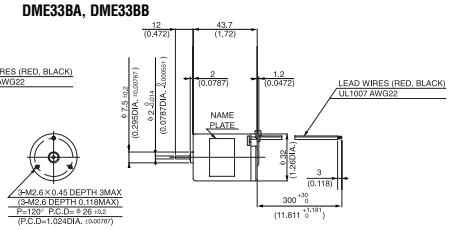

●CURRENT, SPEED-TORQUE CURVE

DME33SA, DME33SB

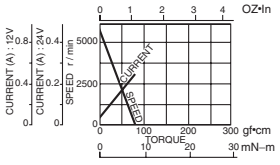

DME33BA, DME33BB

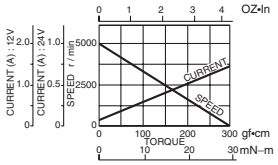

●CONNECTION

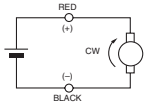

●STANDARD SPECIFICATIONS

Model	Rated						No load		Stall torque		Weight	
	Output	Voltage	Torque		Current	Speed	Current	Speed	mN-m	oz-in		
	W	V	mN-m	oz-in	A	r/min	A	r/min			g	lb
DME33SA	0.7	12	1.5	0.21	0.12	4500	0.05	5500	7.8	1.11	70	0.15
DME33SB	0.7	24	1.5	0.21	0.06	4500	0.02	5500	7.8	1.11	70	0.15
DME33BA	3	12	7.8	1.11	0.42	3700	0.06	5000	29	4.17	100	0.22
DME33BB	3	24	7.8	1.11	0.22	3700	0.04	5000	29	4.17	100	0.22

●REVOLUTION SENSOR MAGNET TYPE

DME33SMA, DME33SMB

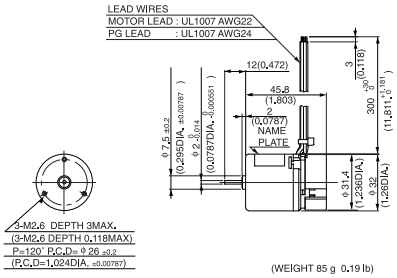

(WEIGHT 85 g 0.19 lb)

DME33BMA, DME33BMB

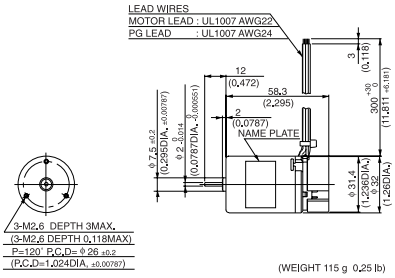

(WEIGHT 115 g 0.25 lb)

●CONECTION OF REVOLUTION SENSOR

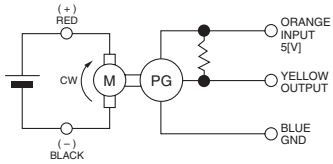

●SPECIFICATION OF REVOLUTION SENSOR SHOWN ON PAGE 8.

Bibliography

[1] Iraide López et al. "Review of wave energy technologies and the necessary power-equipment." In: *Renewable and sustainable energy reviews* 27 (2013), pp. 413–434.

[2] Peter Meisen and Alexandre Loiseau. "Ocean energy technologies for renewable energy generation." In: *Global Energy Network Institute* (2009).

[3] Tri Dung Dang, Cong Binh Phan, and Kyoung Kwan Ahn. "Design and investigation of a novel point absorber on performance optimization mechanism for wave energy converter in heave mode." In: *International Journal of Precision Engineering and Manufacturing-Green Technology* (2019), pp. 1–12.

[4] Richard Boud. "Wave and Marine Current Energy; status and research and development priori-ties." In: *Future Energy Solutions for DTI and IEA OES Implementing Agreement, IEA, Paris, France* (2003).

[5] Marcus Lehmann et al. "Ocean wave energy in the United States: Current status and future perspectives." In: *Renewable and Sustainable Energy Reviews* 74 (2017), pp. 1300–1313.

[6] World Energy Council. "World Energy Resources: Marine Energy 2016." In: *World Energy Council* (2016).

[7] Ottmar Edenhofer et al. *Renewable energy sources and climate change mitigation: Special report of the intergovernmental panel on climate change*. Cambridge University Press, 2011, pp. 87–88.

[8] Atlantis Resources. *Estimate of global potential tidal resources*. Accessed: 2018-11-29 Available: https://marineenergy.biz/2015/02/17/estimate-of-global-potential-tidal-resources/.

[9] Krishnakumar Rajagopalan and Gérard C Nihous. "Estimates of global Ocean Thermal Energy Conversion (OTEC) resources using an ocean general circulation model." In: *Renewable Energy* 50 (2013), pp. 532–540.

[10] L Mofor, J Goldsmith, and F Jones. "Ocean Energy." In: *Technology Readiness, Patents, Deployment Status and Outlook, International Renewable Energy Agency (IRENA), Abu Dhabi* (2014).

[11] Chi-Yu Li et al. "Experimental Study on the Effects of External Electrical Resistance on the Efficiency of a Point Absorber Wave Energy Converter." In: *The 28th International Ocean and Polar Engineering Conference*. International Society of Offshore and Polar Engineers. 2018.

[12] Hosna Titah-Benbouzid and Mohamed Benbouzid. "An up-to-date technologies review and evaluation of wave energy converters." In: *International Review of Electrical Engineering-Iree* 10.1 (2015), pp. 52–61.

[13] Filippos Kalofotias. "Study for the Hull shape of a wave energy converter-point absorber; design optimization & modeling improvement." MA thesis. University of Twente, 2016.

[14] Arthur Pecher and Jens Peter Kofoed. "Power Take-Off Systems for WECs." In: *Handbook of Ocean Wave Energy*. Springer, 2017, pp. 213–214.

[15] Marc Vantorre, Robert Banasiak, and Ronny Verhoeven. "Modelling of hydraulic performance and wave energy extraction by a point absorber in heave." In: *Applied Ocean Research* 26.1-2 (2004), pp. 61–72.

[16] Elie Al Shami, Ran Zhang, and Xu Wang. "Point Absorber Wave Energy Harvesters: A Review of Recent Developments." In: *Energies* 12.1 (2019), p. 47.

[17] Cecilia Boström and Mats Leijon. "Operation analysis of a wave energy converter under different load conditions." In: *IET Renewable Power Generation* 5.3 (2011), pp. 245–250.

[18] KK Ahn et al. "An innovative design of wave energy converter." In: *Renewable Energy* 42 (2012), pp. 186–194.

[19] Simon Thomas et al. "Performance of a Direct-Driven Wave Energy Point Absorber with High Inertia Rotatory Power Take-off." In: *Energies* 11.9 (2018), p. 2332.

[20] João Cruz. *Ocean wave energy: current status and future prespectives*. Springer Science & Business Media, 2007.

[21] Benjamin Drew, Andrew R Plummer, and M Necip Sahinkaya. *A review of wave energy converter technology*. 2009.

[22] Kester Gunn and Clym Stock-Williams. "Quantifying the global wave power resource." In: *Renewable Energy* 44 (2012), pp. 296–304.

[23] *World Power consumption. Electricity consumption. Enerdata*. URL: `https://yearbook.enerdata.net/electricity/electricity-domestic-consumption-data.html`.

[24] Albatern Ltd. *Wave Energy Potential*. URL: http://albatern.co.uk/wave-energy/.

[25] MJ French. "On the difficulty of inventing an economical sea wave energy converter: a personal view." In: *Proceedings of the Institution of Mechanical Engineers, Part M: Journal of Engineering for the Maritime Environment* 220.3 (2006), pp. 149–155.

[26] Giacomo Vissio. "ISWEC toward the sea - Development, Optimization and Testing of the Device Control Architecture." PhD thesis. Politecnico di Torino, 2017.

[27] Kathleen A. Edwards and Mike Mekhiche. "Ocean Power Technologies Powerbuoy®: System-Level Design, Development and Validation Methodology." In: 2014.

[28] Ross Henderson. "Design, simulation, and testing of a novel hydraulic power take-off system for the Pelamis wave energy converter." In: *Renewable energy* 31.2 (2006), pp. 271–283.

[29] Mattia Raffero et al. "Stochastic control of inertial sea wave energy converter." In: *The Scientific World Journal* 2015 (2015).

[30] AWS Ocean Energy Ltd. *ARCHIMEDES WAVESWING SUBMERGED WAVE POWER BUOY*. URL: http://www.awsocean.com/archimedes-waveswing.html.

[31] Aquamarine Power. *Oyster, the wave power harvester from Aquamarine Power*. URL: http://www.blokeish.com/2009/12/experimental-devices-harness-wavepower/.

[32] Giovanna Bevilacqua and Barbara Zanuttigh. "Overtopping Wave Energy Converters: general aspects and stage of development." In: (2011).

[33] Ted Brekken, Belinda Batten, and Ean Amon. "From blue to green [ask the experts]." In: *IEEE Control Systems* 31.5 (2011), pp. 18–24.

[34] AW-Energy. *WAVEROLLER*. URL: http://aw-energy.com/waveroller/.

[35] Wave Star A/S. *Wavestar machine*. URL: http://wavestarenergy.com/.

[36] Aquamarine Power. *AQUAMARINE POWER*. URL: http://www.emec.org.uk/about-us/wave-clients/aquamarine-power/.

[37] Eco Wave Power. *Gibraltar Project*. URL: https://www.ecowavepower.com/gallery/photos/.

[38] Inc Ocean Power Technologies. *POWERBUOY TECHNOLOGY*. Accessed: 2019-02-07 Available: https://www.oceanpowertechnologies.com/media.

[39] EMEC. *PELAMIS WAVE POWER*. URL: http://www.emec.org.uk/about-us/wave-clients/pelamis-wave-power/.

[40] SEABASED. *SEABASED TECHNOLOGY*. URL: https://www.seabased.com/the-technology.

[41] António F. de O. Falcão. "Wave energy utilization: A review of the technologies." In: *Renewable and Sustainable Energy Reviews* 14.3 (2010), pp. 899 – 918. ISSN: 1364-0321. DOI: https://doi.org/10.1016/j.rser.2009.11.003. URL: http://www.sciencedirect.com/science/article/pii/S1364032109002652.

[42] Yuanrui Sang et al. "Resonance control strategy for a slider crank WEC power take-off system." In: *Oceans-St. John's, 2014*. IEEE. 2014, pp. 1–8.

[43] Emmanuel B. Agamloh, Alan K. Wallace, and Annette von Jouanne. "A novel direct-drive ocean wave energy extraction concept with contact-less force transmission system." In: *Renewable Energy* 33.3 (2008), pp. 520 –529. ISSN: 0960-1481. DOI: https://doi.org/10.1016/j.renene.2007.01.008. URL: http://www.sciencedirect.com/science/article/pii/S0960148107000274.

[44] Changwei Liang, Junxiao Ai, and Lei Zuo. "Design, fabrication, simulation and testing of an ocean wave energy converter with mechanical motion rectifier." In: *Ocean Engineering* 136 (2017), pp. 190 –200. ISSN: 0029-8018. DOI: https://doi.org/10.1016/j.oceaneng.2017.03.024. URL: http://www.sciencedirect.com/science/article/pii/S0029801817301312.

[45] K. L. De Koker et al. "Modeling of a power sharing transmission in a wave energy converter." In: *2016 IEEE 16th International Conference on Environment and Electrical Engineering (EEEIC)*. June 2016, pp. 1–5. DOI: 10.1109/EEEIC.2016.7555558.

[46] B. C. Boren et al. "Design, Development, and Testing of a Scaled Vertical Axis Pendulum Wave Energy Converter." In: *IEEE Transactions on Sustainable Energy* 8.1 (Jan. 2017), pp. 155–163. ISSN: 1949-3029. DOI: 10.1109/TSTE.2016.2589221.

[47] Riku Takaramoto, Masashi Kashiwagi, Katsuhiro Sakai, et al. "Wave energy absorption in irregular waves by a floating body equipped with interior rotating electric-power generator." In: *The Twenty-fourth International Ocean and Polar Engineering Conference*. International Society of Offshore and Polar Engineers. 2014.

[48] Youming Dai, Yangzhi Chen, and Longhan Xie. "A study on a novel two-body floating wave energy converter." In: *Ocean Engineering* 130 (2017), pp. 407 – 416. ISSN: 0029-8018. DOI: https://doi.org/10.1016/j.oceaneng.2016.11.049. URL: http://www.sciencedirect.com/science/article/pii/S0029801816305546.

[49] Kesayoshi Hadano, Ki Yeol Lee, and Byung Young Moon. "A study on dynamic motion and wave power in multi-connected wave energy converter." In: *Ships and Offshore Structures* 11.7 (2016), pp. 679–687.

[50] Byung-Ha Kim et al. "Numerical and experimental studies on the PTO system of a novel floating wave energy converter." In: *Renewable energy* 79 (2015), pp. 111–121.

[51] Daniel Wallace, H Bora Karayaka, and Yazan Alqudah. "Optimum parameter search for a slider-crank wave energy converter under regular and irregular wave conditions." In: *SoutheastCon 2017*. IEEE. 2017, pp. 1–7.

[52] Yuanrui Sang et al. "A rule-based phase control methodology for a slider-crank wave energy converter power take-off system." In: *International journal of marine energy* 19 (2017), pp. 124–144.

[53] Yuanrui Sang et al. "Irregular wave energy extraction analysis for a slider crank WEC power take-off system." In: *2015 Intl Aegean Conference on Electrical Machines & Power Electronics (ACEMP), 2015 Intl Conference on Optimization of Electrical & Electronic Equipment (OPTIM) & 2015 Intl Symposium on Advanced Electromechanical Motion Systems (ELECTROMOTION)*. IEEE. 2015, pp. 348–354.

[54] A. K. Laing et al. *Guide to wave analysis and forecasting*. 1998. ISBN: 9263127026.

[55] Pedro Jorge Borges Fontes Negrao Beirao and Cândida Maria dos Santos Pereira Malça. "Design and analysis of buoy geometries for a wave energy converter." In: *International Journal of Energy and Environmental Engineering* 5.2-3 (2014), p. 91.

[56] A Hulme. "The wave forces acting on a floating hemisphere undergoing forced periodic oscillations." In: *Journal of Fluid Mechanics* 121 (1982), pp. 443–463.

[57] Robert L Norton and Sid Shih-Liang Wang. *Design of machinery: an introduction to the synthesis and analysis of mechanisms and machines*. McGraw-Hill Higher Education, 2004.

[58] Hamid D Taghirad. *Parallel robots: mechanics and control*. CRC press, 2013.

[59] Haim Baruh. *Analytical dynamics*. WCB/McGraw-Hill Boston, 1999.

[60] Stephen Chapman. *Electric machinery fundamentals*. Tata McGraw-Hill Education, 2005.

[61] Festo Didactic Ltée/Ltd. *Electricity and New Energy Permanent Magnet DC Motor*. 2014. ISBN: 9782896405053.

[62] Benjamin C Kuo and Farid Golnaraghi. *Automatic control systems*. Vol. 9. Prentice-Hall Englewood Cliffs, NJ, 1995.

[63] Thomas Coleman, Mary Ann Branch, and Andrew Grace. "Optimization toolbox." In: *For Use with MATLAB. User's Guide for MATLAB 5, Version 2, Relaese II* (1999).

[64] SIMPLIFY3D. *PLA*. URL: `https://www.simplify3d.com/support/materials-guide/pla/`.

[65] Amelie Tetu, Miguel Lopes, and Sylvain Bourdier. "Report on Instrumentation Best Practice: WP2: Marine Energy System Testing-Standardisation and Best Practice." In: (2013).

[66] Tristan Pérez and Thor I Fossen. "Time-vs. frequency-domain identification of parametric radiation force models for marine structures at zero speed." In: *Modeling, Identification and Control: A Norwegian Research Bulletin* 29.1 (2008), pp. 1–19.

[67] CT Stansberg et al. "The specialist committee on waves final report and recommendations to the 23rd ITTC." In: *Proceedings of the 23rd ITTC* 2 (2002), pp. 505–551.